(2)

A TRIDENT SCHOLAR PROJECT REPORT

NO. 181

"DEFECTS IN CALCITE"

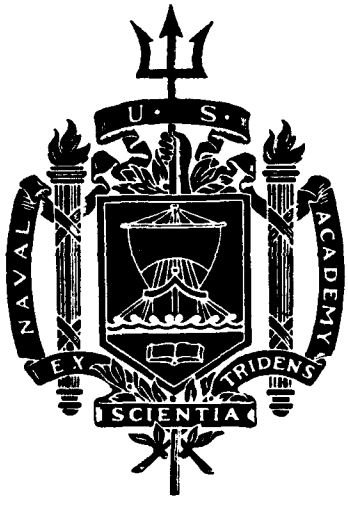

UNITED STATES NAVAL ACADEMY
ANNAPOLIS, MARYLAND

"DEFECTS IN CALCITE"

A Trident Scholar Project Report

by

Midshipman Anthony J. Kotarski, Class of 1991

U. S. Naval Academy

Annapolis, Maryland

Associate Professor Mary C. Wintersgill
Physics Department

Assistant Professor Joseph F. Lomax
Chemistry Department

Accepted for Trident Scholar Committee

Francis D Correll
Chair

13 May 1991
Date

REPORT DOCUMENTATION PAGE

Form Approved
OMB No 0704-0188

1. AGENCY USE ONLY (Leave blank)	2. REPORT DATE	3. REPORT TYPE AND DATES COVERED
	13 May 1991	Final 1990/91

4. TITLE AND SUBTITLE
DEFECTS IN CALCITE

5. FUNDING NUMBERS

6. AUTHOR(S)
Anthony J. Kotarski

7. PERFORMING ORGANIZATION NAME(S) AND ADDRESS(ES)
U.S. Naval Academy, Annapolis, MD

8. PERFORMING ORGANIZATION REPORT NUMBER
U.S.N.A. - TSPR; 181 (1991)

9. SPONSORING/MONITORING AGENCY NAME(S) AND ADDRESS(ES)

10. SPONSORING/MONITORING AGENCY REPORT NUMBER

11. SUPPLEMENTARY NOTES
Accepted by the U.S. Trident Scholar Committee.

12a. DISTRIBUTION/AVAILABILITY STATEMENT
This document has been approved for public release; its distribution is UNLIMITED.

12b. DISTRIBUTION CODE

13. ABSTRACT (Maximum 200 words)

Audio frequency complex impedance measurements have been carried out in vacuum over the temperature range 5.5-300K on three types of naturally occurring calcite samples. The measurements were made with the electric field perpendicular to the cleavage planes and both parallel and perpendicular to the c axis. All materials exhibit a 1000 Hz relaxation peak parallel to the optic axis with a peak position of about 38K. This relaxation is strongest in the Swakopmund (blue) calcite and appears to be associated with an yttrium-(CO_3)-3 ion pair. The Gallatin (yellow) and Iceland Spar (clear) samples show a relaxation at very low temperatures perpendicular to the c axis (7K at about 1000 Hz) which exhibits characteristics of a tunnelling phenomenon that is attributed to proton motion. Five other relaxations are observed and their possible origins are discussed. Determinative analysis of the calcites was performed by using the following experimental methods: X-ray fluorescence, atomic absorption, optical absorption, neutron activation analysis, Fourier transform infrared analysis, and radiative bombardment. The theory, techniques, and results of these methods are briefly discussed.

14. SUBJECT TERMS
Calcite
Dielectric relaxation
Dielectric loss

15. NUMBER OF PAGES
118

16. PRICE CODE

17. SECURITY CLASSIFICATION OF REPORT	18. SECURITY CLASSIFICATION OF THIS PAGE	19. SECURITY CLASSIFICATION OF ABSTRACT	20. LIMITATION OF ABSTRACT
UNCLASSIFIED	UNCLASSIFIED	UNCLASSIFIED	

ABSTRACT

Audio frequency complex impedance measurements have been carried out in vacuum over the temperature range 5.5-300 K on three types of naturally occurring calcite samples. The measurements were made with the electric field perpendicular to the cleavage planes and both parallel and perpendicular to the *c* axis. All materials exhibit a 1000 Hz relaxation peak parallel to the optic axis with a peak position of about 38K. This relaxation is strongest in the Swakopmund (blue) calcite and appears to be associated with an yttrium-$(CO_3)^{-3}$ ion pair. The Gallatin (yellow) and Iceland Spar (clear) samples show a relaxation at very low temperatures perpendicular to the *c* axis (7K at about 1000 Hz) which exhibits characteristics of a tunnelling phenomenon that is attributed to proton motion. Five other relaxations are observed and their possible origins are discussed. Determinative analysis of the calcites was performed by using the following experimental methods: X-ray fluorescence, atomic absorption, optical absorption, neutron activation analysis, Fourier transform infrared analysis, and radiative bombardment. The theory, techniques, and results of these methods are briefly discussed. Finally, dielectric analysis of vanadyl phosphate dihydrate has additionally been performed. The effect which the hydrates had on the dielectric properties of the material is discussed.

LIST OF CONTENTS

LIST OF FIGURES

LIST OF TABLES

1. INTRODUCTION:

In its various forms, calcite is one of the most widely distributed of minerals. It is a major constituent of the sedimentary rocks and a minor constituent (of secondary origin) of the igneous rocks. Deposited in caves by lime-bearing waters, calcite takes the form of stalactites, stalagmites, and crystalline encrustations.[1] Additionally, metamorphic marble and limestone both consist of very small interlocking calcite crystals.[2] Although it has drawn some minor technological interest as a stable birefringent material with a high dielectric constant, the majority of research involving calcite over the past few years has focused mainly upon the anisotropic crystalline properties of the pure material. A systematic study of the defect complexes has not been conducted up to this point. Such a study would be of great geological interest since the presence of defects in natural minerals is inevitable. A knowledge of their characteristics would help to describe their properties. The objective of this research was to examine and study the nature and configuration of the more prevalent defect complexes that commonly occur in a variety of calcite samples. Theoretical models for the complexes have been postulated.

A number of different analytical techniques were employed in the investigation of the defect complexes in calcite. Dielectric relaxation measurements comprised the heart of this project. Other analytical techniques used will be treated as separate experiments. The role which each of those experiments played in the grand scheme of postulating defect complexes will be brought together in Section 8.6, which discusses the experimental evidence that led to the postulation of specific defect complexes.

Additional dielectric studies were performed on vanadyl phosphate dihydrate in order to quantitatively and qualitatively determine how the hydrates affected the properties of the vanadyl phosphate. This work was a small part of an ongoing study conducted by Joseph F. Lomax, Chemistry Department, U.S. Naval Academy, on the characteristics of ion movement in vanadyl pnictates and their intercalation compounds.

2. CALCITE BACKGROUND:

In its pure form, calcite is a colorless uniaxial substance having nearly parallel dispersion curves, a very high negative, and a space group of D_{3d}^{6}.[3] Its structure consists of alternating planes of Ca^{+2} cations and $(CO_3)^{-2}$ anions. The $(CO_3)^{-2}$ anion is a trigonal planar arrangement of a carbon atom surrounded by three larger oxygen ions. Both ionic planes are perpendicular to the crystallographic *c* (optic) axis [0001] and therefore exhibit nearly perfect rhombohedral cleavage. This is attributed to the fact that bonding forces are weak across the planes parallel to the faces of the crystal rhombohedron.[4] The cleavage face is in the $[10\bar{1}1]$ plane, and its normal intersects the *c* axis at an angle of 44°36'. Figure 2.1 shows both the true primitive cell and the cleavage pseudocell of calcite. The primitive cell is the smallest naturally occurring microscopic building block of the calcite, and the cleavage pseudocell is the macroscopic structure which results when large numbers of primitive cells join together. Naturally occurring calcite cleaves from Montana (Gallatin Mountain), Southwest Africa (Swakopmund), and Mexico (Creel, Chihuahua) were obtained from Ward's Natural Science Establishment, Inc. of Rochester, New York.

Figure 2.1. The crystal structure of calcite. The elongated cell showing the carbonate and calcium ions is referred to as the true primitive cell of the crystal. The rhombohedron is referred to as the cleavage pseudocell of the crystal.

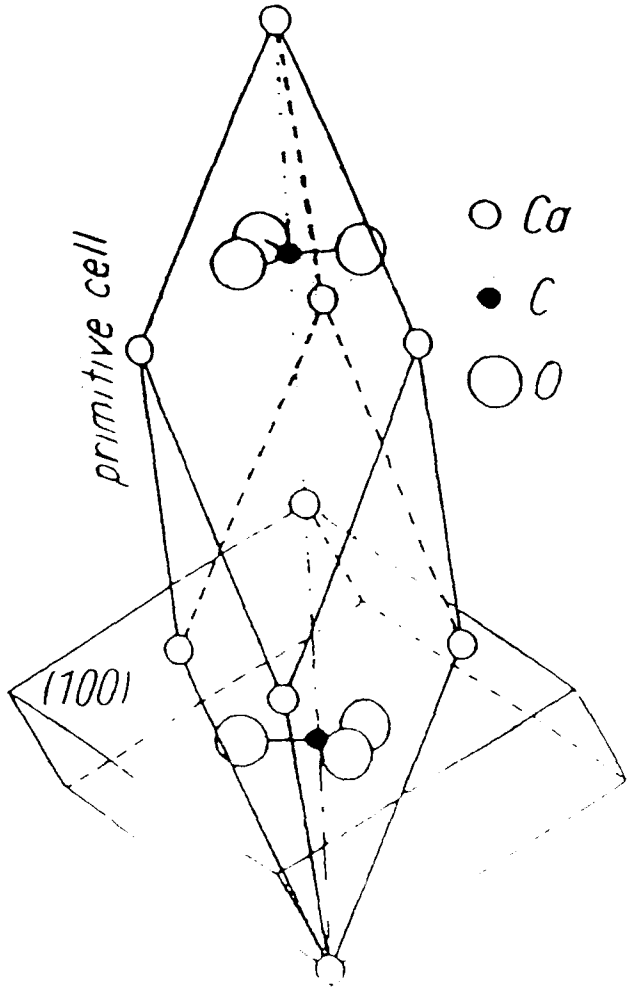

The Swakopmund samples were of a bluish-white marble color with an opaque nature; the Mexican samples were of the clear Iceland Spar variety; and the Gallatin samples were of a faint yellow color with only a slightly opaque nature.

3. X-RAY FLUORESCENCE:

3.1 Introduction: X-ray fluorescence operates on the principle that elements will emit radiation in the form of X-rays when they are excited as described in the following section. These radiations can then be used to deduce both the type and concentration of trace elements present in various samples. Present X-ray spectographs are capable of detecting elemental concentrations of several parts per billion.[5] X-ray fluorescence is a very rapid experimental technique with many advantages. It is non-destructive and extremely amenable to automation. However, in this case X-ray fluorescence will be used as a very rapid method of determining the elementary impurity makeup of the calcite samples.

3.2 Theory: When an atom absorbs a sufficient amount of energy, excited electrons may be ejected from its innermost shells. These vacancies are filled by electrons from the outer shells within a time period of about 10^{-15} seconds. In the process of transiting to the inner shell, the outer-shell electrons will give up energy in the form of photons of electromagnetic radiation. In the X-ray region, the wavelength of these photons typically ranges from 0.1 through 70 Å. The energy and associated wavelengths of the photons are given by the relationship[6]:

$$E = \left| E_{OUTER} - E_{INNER} \right| = \frac{h\,c}{\lambda} \qquad (3.1)$$

where E is the photon energy, c is the velocity of light, h is Planck's constant, and λ is the wavelength of the secondary X-radiation generated. The X-ray spectrum is divided into different series. They begin with the K, L, M, N, . . . series which results from vacancies spaces in the K, L, M, N, . . . shells, respectively. The relative intensities of the emission lines from a given series are a result of different transitional probabilities. Usually, the transitions are represented by lines on an energy level diagram. The wavelength of a characteristic line is related to atomic number Z by Moseley's Law:

$$\frac{1}{\lambda} = K(Z - \sigma)^2 \qquad (3.2)$$

in which K and σ are constants which depend upon the particular series of radiation.[6] Because the electron energies in the atoms of a certain element are fixed, E may only assume a limited number of values that are characteristic of each element. The identity of trace element impurities are determined in this way. Additionally, the relative intensities of different lines provide information on the concentration of trace impurities. Mixtures of elements will produce simple additive spectra.

3.2 Experiment: Non-invasive X-ray fluorescence analysis was performed using a Kevex 0750 unit. The X-ray beam was collimated to 6 mm. The unit was configured for a molybdenum target. Barium served as a secondary target. The voltage was set at 60 kV, and the current was 40 mA. Irradiations were performed at the Scientific Research Department of the National Gallery of Art in Washington, D.C. Irradiation time for each

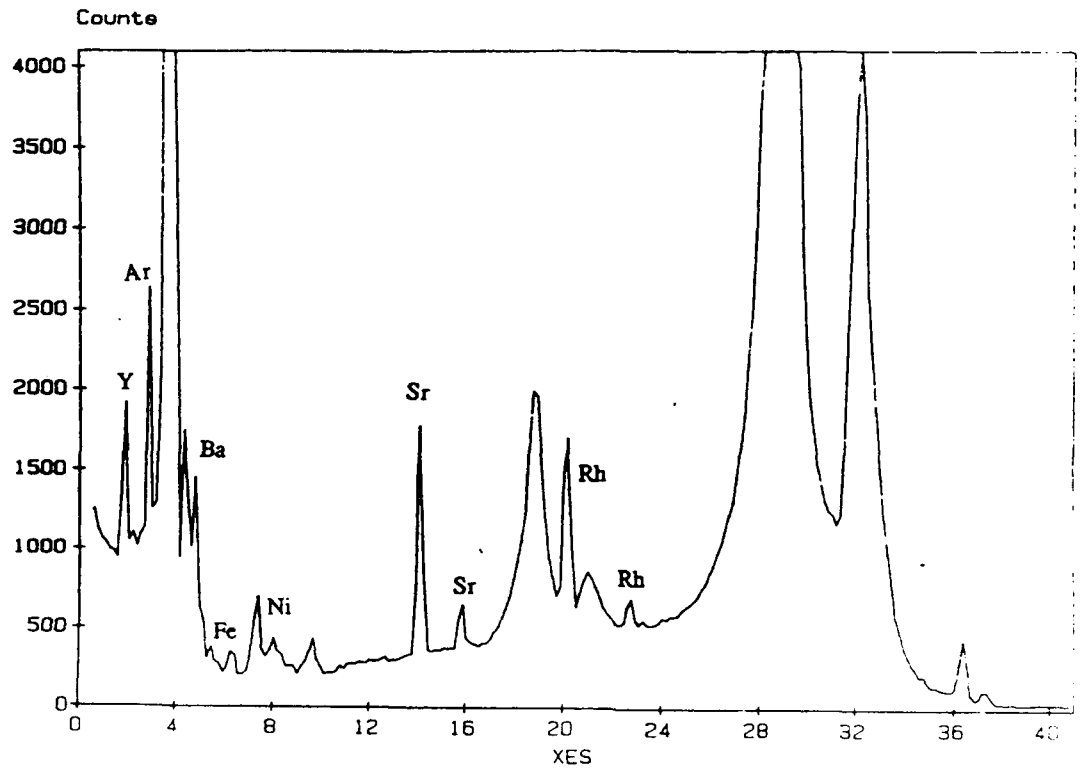

Figure 3.1. The number of counts per channel versus energy in keV of characteristic X-rays in the Swakopmund calcite. The sample was bombarded with X-rays using a barium target for a time interval of 527 seconds.

sample varied from 240-600 real-time seconds. Samples were irradiated only long enough to be able to distinguish characteristic emission lines from background counts. Therefore, only qualitative analysis of the elements was possible.

3.3 Results: Figure 3.1 shows the resulting plot of the number of counts versus energy for the Swakopmund sample using a barium target crystal. The energy values and corresponding line transitions are listed in Table 3.1. Similar plots were constructed for the Iceland Spar and Gallatin samples. The very narrow, very high peak on the left of the spectrum corresponds to calcium. The two broad peaks to the right of the spectrum result from Rayleigh and Compton scattering of the incoming X-ray beam by the sample.[5] The peaks seen in the plots represent characteristic electron transitions in the atoms of the samples.

Table 3.1. Characteristic X-ray fluorescence energy values and transitional lines seen in Swakopmund calcite configured with a barium crystal target. The sample was irradiated for 527 seconds.

Element	Energy (keV)	Transitional Line
Yttrium(Y)	2.369	$L_{I\,\alpha\beta}$
Argon(Ar)	3.191	K_{β}
Barium(Ba)	4.828	$L\beta^1$
	5.531	$L\gamma^1$
Nickel(Ni)	7.460	$K\alpha^2$
	8.264	$K\beta^1$
Strontium(Sr)	14.097	$K\alpha^2$
	15.834	$K\beta^1$
Rhodium(Rh)	20.214	$K\alpha^1$
	23.169	$K\beta^2$

Collectively, trace amounts of argon, yttrium, manganese, zinc, copper, nickel, iron, strontium, barium, molybdenum, and rhodium were determined to be present in the samples. However, the argon, barium, and molybdenum peaks observed in the spectra probably were not caused by the presence of these elements in the samples. Transitions for argon appeared as a result of X-rays interacting with the air surrounding the sample target. The barium and molybdenum transitions result from the respective target crystals used in the experimental apparatus.[7] A listing of the elements found in each calcite sample is given in Table 3.2. Only strontium, nickel, yttrium, and iron appear in all three samples. Additionally, each sample possesses one unique impurity which no other sample shares. This impurity is rhodium in the Swakopmund sample. In the Iceland Spar and Gallatin calcites, the unique trace impurities are zinc and manganese, respectively.

Table 3.2. Trace impurities found in Swakopmund, Iceland Spar, and Gallatin calcites using X-ray fluorescence. The symbol * denotes the confirmed presence of the trace element.

Sample	Y	Mn	Zn	Cu	Ni	Fe	Sr	Rh
Swakopmund	*			*	*	*	*	*
Iceland Spar	*		*	*	*	*	*	
Gallatin	*	*			*	*	*	

3.4 Discussion: Because calcite is a naturally occurring mineral, it is suspected to have a number of defect complexes associated with its crystal lattice. More often than not, these defect complexes result from trace elemental impurities incorporated into the lattice when the crystal forms. Although X-ray fluorescence may be a useful quantitative tool when

performed and analyzed in a very precise manner, for the purposes of this study its use was chiefly limited to qualitative analysis. Hence, X-ray fluorescence was used to establish a qualitative spectrum of trace elements present in the calcites. This spectrum was then used as a guideline while performing much more exact, quantitative methods of elemental analysis such as atomic absorption and neutron activation analysis.

The spectrum of impurities obtained from X-ray fluorescence agrees well with published results. Manganese, iron, cobalt, magnesium, aluminum, silicon[8], sodium, lithium, and cadmium[9] are considered to be the most common impurities found in calcite. It has already been noted that the Gallatin calcite is the only sample which contains manganese. As mentioned in Section 2, Gallatin calcite has a brownish-yellow color and is slightly opaque. Published results attribute this yellow hue of natural calcites to manganese impurities.[10] Basing expectations on sample color alone, Iceland Spar calcite was thought to be the most pure of the three samples due to its clear, colorless appearance. Similarly, Swakopmund calcite was expected to contain higher concentrations of impurities. The data appearing in Table 3.2 lends support to this observation. The Iceland Spar, Gallatin, and Swakopmund samples contain 5, 6, and 7 trace impurities, respectively.

No cobalt, magnesium, aluminum, silicon, sodium, lithium, or cadmium has been detected using this technique for two reasons. First and foremost, X-ray fluorescence was performed in a qualitative, not quantitative manner. For the purposes of this study, it would not have been expedient to scan the samples as thoroughly as more precise analysis would require. The software necessary for data reduction is not on hand at the U.S. Naval Academy, making extensive analysis quite difficult. Secondly,

X-ray fluorescence is not the preferred method of detection for many of the listed elements. Some are difficult to activate through X-ray bombardment and are more easily detected through other determinative methods such as thermoluminescence, for example.

3.5 Conclusion: X-ray fluorescence measurements were performed on all of the calcite samples in order to establish a very rudimentary, qualitative analysis of elemental impurities. Traces of yttrium, manganese, zinc, copper, nickel, iron, strontium, and rhodium were identified. This spectrum will furnish the information needed to conduct more quantitative analysis techniques that require previous knowledge of sample impurity content, i.e., atomic absorption. The results of these methods will additionally be compared to those of X-ray fluorescence to check for consistency. Similarly, just knowing which element appeared in what sample will greatly facilitate determining the existing correlations between dielectric loss and the trace impurities present.

4. ATOMIC ABSORPTION:

4.1 Introduction: Atomic absorption is a powerful tool employed by chemical analysts to quantify trace concentrations of impurities. The technique is based on the ability of vaporized atoms to absorb energy from a characteristic beam of light of suitable wavelength. The percent transmission or absorbance of unknown atomized solutions are measured and then compared to those of known standard concentrations to determine how much of a specific element is present within a sample.[11] Previous knowledge of the sample's rudimentary impurity spectrum is required so that the proper standard solutions may be prepared. Atomic absorption is

an ideal technique for calcite analysis because of the small amount of sample needed (atomic absorption is a destructive technique). Additionally, all calcites dissolve readily in nitric acid (HNO_3) solutions, which are typically used in atomic absorption. Based on the results of X-ray fluorescence and the equipment on hand at USNA, only tests for copper, zinc, nickel, and iron will be conducted with atomic absorption.

Typical absorption spectrophotometers are comprised of three main sections: the light source, the absorption flame or furnace, and the wavelength selector and detector. The light sources are usually hollow cathode lamps capable of producing a line spectrum specific to the element being determined. Each element being analyzed requires its own lamp. The absorption flame or furnace functions to atomize the sample solution. Flame or furnace methods must be as constant as possible to produce reliable results. Wavelength selection and detection is accomplished by either an optical grating or a prism and a slit system. Only a narrow band of wavelength will reach the detector for final transmission. This minimizes the effects produced by the general absorptivity of the flame or furnace. Detector units incorporate photomultipliers to produce a digital output.[5]

4.2 Theory: Atomizing furnaces produce analytical signals which are transient in nature. Two parameters may be proportional to the amount of analyte: the peak height or the peak area. Peak area will not be discussed. Peak height refers to the magnitude of the highest part of the output signal observed with time during the atomization portion of the cycle. A typical furnace atomic absorption signal may be seen in Figure 4.1.

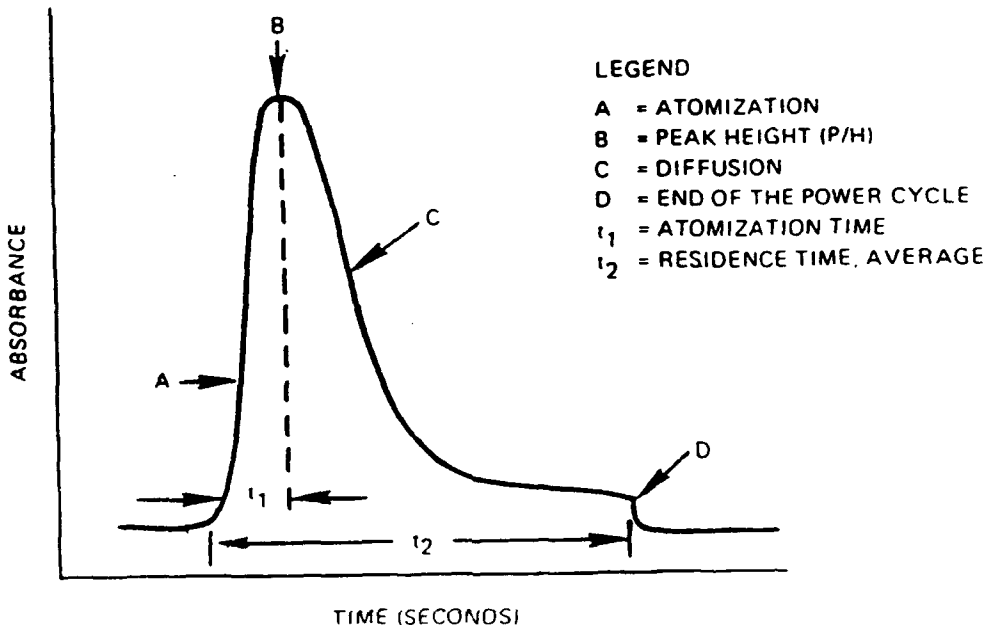

Figure 4.1. A typical atomic absorption signal resulting from furnace atomization.

For the absorbance peak height:

$$N_{peak} = (N_o t_2/t_1) \{1 - \exp(-t_1/t_2)\} \qquad (4.1)$$

where N_{peak} is the number of analyte atoms present at the peak signal, and N_o is the number of analyte atoms injected into the furnace. The atomization time and the residence time of the analyte atom in the observation volume are represented by t_1 and t_2, respectively. If $t_1/t_2 << 1$, then:

$$1 - \exp(-t_1/t_2)) \cong t_1/t_2$$

implying that

$$N_{peak} \cong N_o \qquad (4.2)$$

and therefore a peak height measurement is valid as a measure of the amount of analyte in the sample.[12]

4.3 Experiment: All glassware used was washed once with soap, three times with distilled water, three times with de-ionized water, once with 1:5 HNO_3:H_2O, and then three times with de-ionized water, in that sequence. De-ionized water having a resistance of no less that 10.0 MΩ was used for all dilutions throughout the duration of the experiment. Standard solutions for iron, zinc, nickel, and copper were prepared by dissolving specific amounts of the respective elements in HNO_3 and then diluting to a desired concentration. Table 4.1 lists the concentrations of the standard solutions used.

Table 4.1. Concentrations of the standard solutions used in atomic absorption. All solutions were made with nitric acid.

Element	Concentrations (x 10^{-10} g/mL)
Fe	30, 2, 0.3
Ni	30, 15, 2
Cu	8, 5, 0.2
Zn	0.1 , 0.05

Solutions of Iceland Spar, Gallatin, and Swakopmund were made similarly by dissolving 0.9862 g, 0.6480 g, and 1.0151 g into 10.0 mL of 1:5 HNO_3:H_2O, respectively. The solutions were diluted to concentrations which fell within the working range of the spectrophotometer used.

The experimental apparatus consisted of an Instrumentations Laboratory Inc. fully automated IL755 furnace atomizer and IL857 aa/ae spectrophotometer. The IL857 was used in double beam mode. Five experimental runs were performed with each unknown and its respective standard to produce mean absorbances. The furnace atomizer and the spectrophotometer were configured for instrumental parameters listed elsewhere.[11] All manual injections were made into the furnace in 25 µL aliquots using 20 and 5 µL fixed volume syringes. Absorption of the light beam occurred within pyro-coated graphite tubes. Separate "blank" runs, using de-ionized water, were made for each element being analyzed. The blank runs functioned to adjust the electronic circuitry so that zero absorbance was correlated with zero concentration.

4.4 Results: From the mean absorbances of the standard solution data runs, plots of absorbance versus concentration were constructed for

each element being tested. The plot for nickel is shown in Figure 4.2. The straight line is a least squares best fit to the plotted data. Trace impurity concentrations were determined graphically using the concentration curves and the known absorbances of the calcite solutions as the entering arguments. The final impurity concentrations were converted into ratios of moles of the trace elements to moles of calcium carbonate. The results appear in Table 4.2. The highest concentration of nickel and zinc appear in the Iceland Spar calcite. Swakopmund and Gallatin calcite had the highest concentrations of copper and iron, respectively. Since the results of X-ray fluorescence showed no zinc to be present in the Swakopmund or Gallatin samples, no tests were even performed for zinc with respect to those samples. The same is true of the copper impurities with regard to the Gallatin calcite.

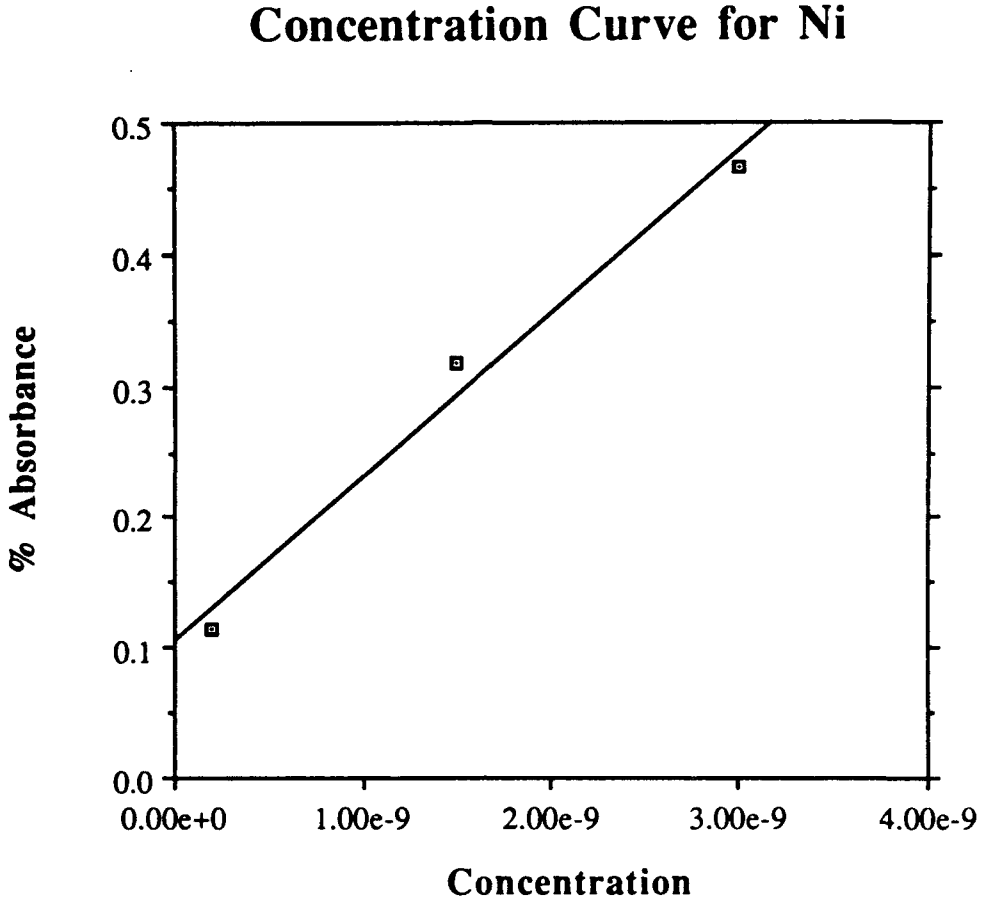

Figure 4.2. Absorbance versus concentration of standard nickel solutions to be used in determining the nickel concentration of various calcites. The standard solutions were prepared using HNO_3. The least squares best fit line is shown.

Table 4.2. Mol (impurity) to mol (calcite) ratios of iron, nickel, copper, and zinc resulting from atomic absorption measurements of Iceland Spar, Swakopmund, and Gallatin calcite solutions.

	Ratio of mol(Xx) to mol ($CaCO_3$) {x 10^{-7}}			
Sample	Fe	Cu	Zn	Ni
Iceland Spar	6.1377	0.3473	1.5567	110.21
Swakopmund	7.2832	1.0183	--------	81.877
Gallatin	17.632	--------	--------	62.489

4.5 Discussion: Published atomic absorption sensitivities for copper, nickel, and iron are on the order of 0.1 parts per million. Zinc has been reported to be detected down to the 0.01 parts per million level.[13] All concentrations calculated through atomic absorption fall well within this minimum sensitivity range. Nevertheless, such results should be interpreted very cautiously. As seen in Table 4.2, many of the concentrations are very close in magnitude. Some additionally differ from published concentration values. In the case of iron, for example, the difference is greater than one order of magnitude.[9]

When performing atomic absorption, one's technique greatly influences one's experimental results. A perfect example of this occurred when testing for zinc in Iceland Spar calcite. While making syringe injections into the graphite furnace, I had absent-mindedly neglected to cap the flask of calcite solution. Unfortunately, construction workers were drilling holes into the cinder block just outside the laboratory. Cinder blocks contain appreciable amounts of zinc. In the time span it took to perform one sample run (2-3 minutes), the zinc absorption of the solution had increased by 100 times due to contamination from cinder block dust in the air.

However, the fact that calcite forms naturally may also account for the discrepancies observed. Because there are such a vast number of natural calcites, each having different physical properties that can be distinguished with the naked eye, one certainly should not expect them all to have roughly the same impurity concentration. Unfortunately, no organized research regarding the impurity spectra of differing natural calcites has been undertaken to this date.

4.6 Conclusion: It was hoped that atomic absorption performed on

the samples would provide a precise impurity concentration to be used in conjunction with the results of dielectric relaxation. Thus, a correlation between impurity content and defect complex properties might then be established. However, the results exhibit poor agreement with published values. Because of the precise experimental technique needed and the many variations of natural calcite samples in existence, the resulting concentrations deduced from atomic absorption are not considered to be very conclusive. Further experimentation with different analytical methods such as optical absorption and neutron activation analysis must be performed. These results can be compared to previous results (atomic absorption and X-ray fluorescence) so that some type of conclusive evidence regarding impurity concentration may be found.

5. OPTICAL ABSORPTION:

5.1 Introduction: Crystals and glasses appear colored because they absorb one or more bands of light whose wavelengths lie in the visible spectrum. When white light is passed through colored crystals and then analyzed by a spectrometer, parts of the original light profile will be "blacked out." These portions correspond to the bands of wavelength which were absorbed by the crystal. By measuring the wavelength at which the absorption occurs, the energy may be calculated and possibly correlated to some type of impurity vibration. In some materials, color may be related to the presence of certain impurity mechanisms; in other materials, it may not. Calcite is a perfect candidate for analysis by optical absorption. Samples may be ground thin enough to allow light to pass through the more opaque crystals. Optical absorption is a very rapid,

accurate, nondestructive technique. The results from this experiment should establish whether or not some of the color mechanisms in calcite are related to impurity content.[14]

5.2 Theory: Light absorptions result from electronic transitions between permitted atomic or molecular energy levels. These electron "jumps" are not very intense because light in the visible and ultra-violet region has a rather low associated photon energy. Jumps will primarily occur among the outermost molecular or atomic levels. These are the same valence levels which are associated with the chemical bonding of the material. Only the highly characteristic nature of these transitions and associated wavelengths allows the property of color to be employed for atomic or molecular identification.[5]

Molecules or atoms can only emit or absorb radiation if their intrinsic energy falls within the specific parameters of some limiting value. Systems of absorbing and/or emitting atoms are assumed to be in a state of dynamic equilibrium. The energy distribution among these atoms is found through the application of Boltzmann statistics. At any temperature, a fraction of the atoms will be in low energy states capable of absorption, and a fraction of the atoms will be in high energy states capable of emission. However, the actual number of atoms that emit and absorb radiation at one instant in time is very small compared to all which are capable of doing so. The number of atoms which do emit or absorb radiation always remains the same for a given system under a set of imposed conditions. Such consistency makes it possible to use optical absorption as an extremely quantitative and comparative tool.[5]

Spectrometers generally measure the extent to which liquid, solid, or gaseous materials absorb light of different wavelengths. Light which

successfully passes through the sample is collected and compared to the intensity of light incident upon the sample by the relationship:

$$I_x = I_o e^{-\kappa x} \qquad (5.1)$$

where I_o and I_x are the intensities of the incident and transmitted light, respectively. Sample thickness is denoted by x, and κ is a constant known as the absorption coefficient. The absorption coefficient is that value by which the fractional reduction in intensity, I_x / I_o, is equal to $e^{-\kappa}$ for each unit of thickness.[14] Light beams used in optical absorption have a selected wavelength and a very narrow waveband.

5.3 Experiment: Measurements were performed using a Varian Model 17 Spectrophotometer scanning wavelengths over a range of 350-650 nm. The scanning rate was 0.5 nm per second and the scanning sensitivity was 15 nm per inch. Measurements were taken at both liquid nitrogen and room temperature. A Cryogenics Associates CT-12 dewar equipped with mylar windows was used for low temperature analysis. Extensive dewar modification was required before it could be used in conjunction with the spectrophotometer. Measurements were performed on both the Swakopmund and the Iceland Spar calcites. The samples were oriented so that the incoming beam ran either perpendicular and parallel to the optic axis. The platelet shaped samples used had already been analyzed dielectrically (another non-destructive technique to be described in Section 8). All samples were ground to a thickness of under 0.80 mm and were polished using 1.0 μm diamond slurry polishing compound.

5.4 Results: The results of optical absorption were null. In other words, no new information was gained about the impurity content of the

samples as a result of this experiment.

5.5 Discussion: Swakopmund was the first crystal to be analyzed. Plots of absorbance versus wavelength were constructed. Because of the sample's blue color, a rather strong absorption band was expected to be observed at or about 600 nm, which is roughly the wavelength of orange/red light. No characteristic absorption bands were observed at all. The mean absorbance over the scanned range varied from 70-80 per cent and was quite noisy. Assuming that the noise was caused by the vibrational motion of atoms in the crystal lattice at room temperature, readings were then performed on the Swakopmund sample at approximately 78 K. The results were the same.

Hence it was assumed that Swakopmund calcite was entirely too opaque to produce any significant results, even when it was ground to such a delicate thickness. Next, data was acquired on Iceland Spar calcite at liquid nitrogen temperatures. Once again, no characteristic absorptions were seen. The mean absorbance of the incident light dropped to approximately 10 per cent in the Iceland Spar calcite. This is attributed to the clear, colorless nature of the sample. Room temperature readings yielded the same results. Experimental procedures were terminated at this point. Although the results of optical absorption analysis were null, they do in fact agree with published results. Studies performed by Lapraz in 1976 have concluded that no significant absorption bands were detected at 290K or 77K for calcite single crystals similar to the ones used in this experiment.[9]

5.6 Conclusion: The results of this experiment have shown absolutely no correlation between those for either atomic absorption or X-ray fluorescence. No significant absorption bands were observed at either

liquid nitrogen or room temperatures. It has been concluded that the mechanisms responsible for color in Swakopmund and Iceland Spar calcite have little or no association with the sample's impurity content.

6. NEUTRON ACTIVATION ANALYSIS:

6.1 Introduction: More information about the impurity content of the calcites is needed. The results of atomic absorption only provide some inconclusive information regarding four elemental impurities. A much wider spectrum of impurities needs to be investigated, and the reproducibility of previous results needs to be evaluated. Neutron activation analysis was employed to accomplish those two objectives.

Experimental procedures involve bombarding a sample with a flux of neutrons. When the incoming neutrons interact with the nuclei of the sample, *radioactive nuclides are formed.* These nuclides will decay with the emission of characteristic radiation at a rate which is well defined for each type of nuclide. Knowledge of the energy emission spectrum and the half life will permit the unambiguous identification of elements that were originally present within the sample at the parts per million level.[15]

6.2 Theory[16]: Activation analysis is based solely upon the interactions of the nuclear force. Entirely unrelated to any chemical properties the sample might possess, activation analysis depends chiefly upon nuclear properties such as nuclear cross sections, half-lives of the product isotopes, and energy emissions of the product isotopes.

In most generators, neutrons are produced when tritium reacts with deuterium to produce helium as shown in Equation 6.1:

$$^{3}_{1}H + ^{2}_{1}H \rightarrow ^{1}_{0}n + ^{4}_{2}He \qquad (6.1)$$

Typical neutron energies range from 13.4 - 14.7 MeV.[17]

Some of the radioactive samples will emit γ rays after being irradiated. The characteristic emission energy of the decaying radionuclides will appear as a peak (commonly referred to as a photopeak) on a plot of counts per channel versus channel number. The number of decay counts under a specific photopeak, known as the integral value (INT), is given by the relationship:

$$INT = \varepsilon \lambda N^{irr} \Omega f_c f_d t_c \qquad (6.2)$$

where ε is the detector efficiency, Ω is the solid angle subtended by the detector, and t_c is the counting time. The terms f_c and f_d both refer to decay corrections which are exponential functions of the decay constant, the counting time, and the decay time. Decay constants are represented by the term λ:

$$\lambda = \frac{\ln 2}{t_{1/2}} \qquad (6.3)$$

where $t_{1/2}$ denotes the half-life of the radionuclide produced. The term N^{irr} represents the number of radioactive atoms present after irradiation has occurred and may be expressed as:

$$N^{irr} = (N_o V)\, \sigma_a \phi \left(1 - e^{-\lambda t_c}\right) \qquad (6.4)$$

where N_o is the initial density of the atoms whose concentration is to be determined, V is the volume of the sample, σ_a is the cross section for the reaction, and ϕ is the flux of the neutron beam used in activation. Detector

efficiencies are calculated by the relationship:

$$\varepsilon = \frac{INT}{I_o\, q\, e^{-\lambda t}\, \Omega\, t_c} \qquad (6.5)$$

where I_o is the initial intensity of the radioactive source (in μCi) that was used for calibration. The branching ratio is given by q, and the term t in the exponential refers to the age of the radioactive source. Solving Equation 6.4 for N_oV results in the following relationship:

$$N_oV = \frac{INT\left(1 - e^{-\lambda t}\right)}{\varepsilon\, \lambda\, \Omega\, \sigma_a\, \phi\, f_c\, f_d\, t_c} \qquad (6.6)$$

where N_oV yields the number of atoms of a specific element present within the sample.

6.3 Experiment: Irradiations were performed with a Kaman Nuclear Model A-711 generator utilizing the $^{3}H(d,n)^{4}He$ reaction. The generator is of the sealed-tube accelerator type capable of producing in excess of 10^{11} 14.3 MeV neutrons per second. Sealed-tube accelerator type neutron generators consist of four parts: a gas reservoir, an ion source, a lens gap to focus and accelerate, and a target for neutron generation. Typically, 5-6 kV are used to ionize the deuterium gas. The ions are accelerated toward the lens with a DC potential of 150 kV. From the lens, they are accelerated even further by an additional 50 kV.[18] Gamma ray detection was accomplished with an Canaberra model GC2019 solid state detector.

The efficiency and energy calibration of the detector were calculated using ^{54}Mn (0.84 MeV), ^{60}Co (1.18 MeV), and ^{137}Cs (1.33 MeV) , and

annihilation (0.511 MeV) photons. A plot of the energy versus channel number for calibration is given in Figure 6.1 Each energy bin was 0.515 keV wide. Readings were taken over 4096 channels covering an energy range of 0-2 MeV.

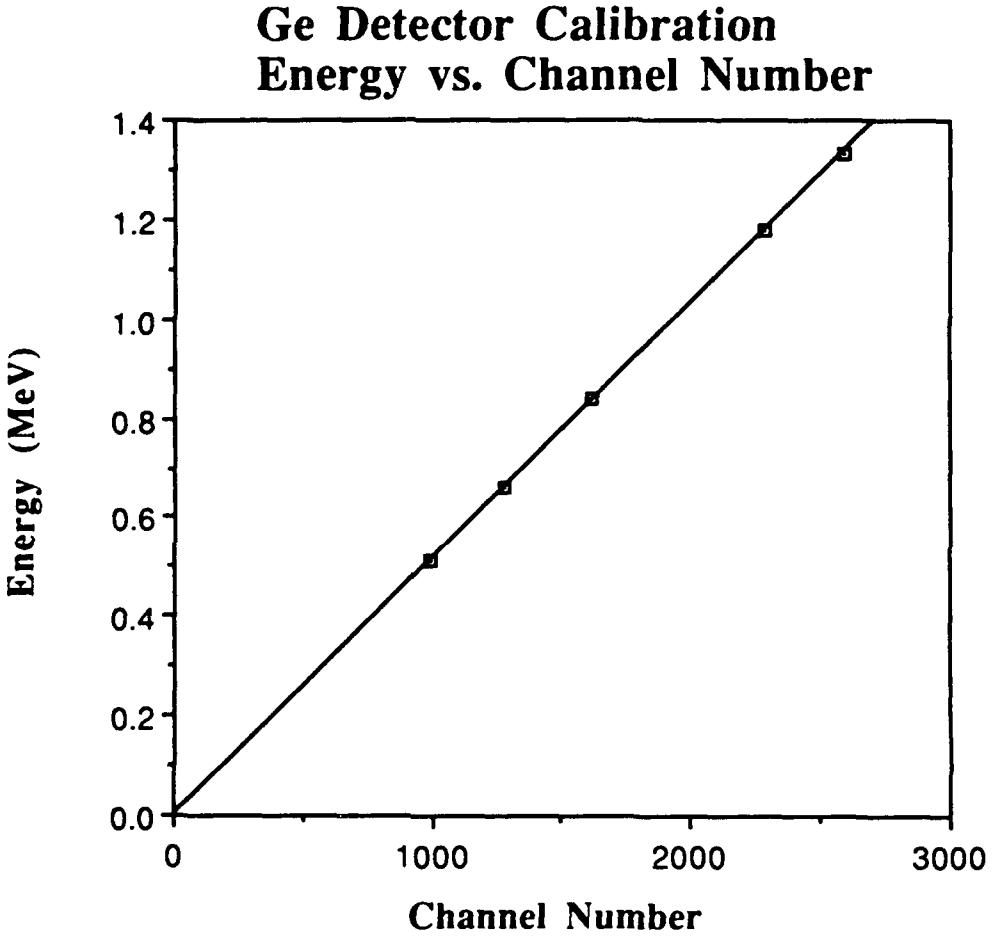

Figure 6.1. Energy versus channel number for the Ge detector used in the Neutron Activation Analysis of calcite. ^{54}Mn, ^{60}Co, ^{137}Cs, and the annihilation peak corresponding to 0.511 MeV were used as points for calibration. The line represents the least squares best linear fit.

The calcite samples were placed in a cadmium box and irradiated to saturation (approximately 15 minutes for the nuclides being investigated).

Readings of the γ ray spectrum were acquired in two 1200 second intervals with 300 seconds elapsing between each data acquisition period. A 1200 second background run was additionally acquired and subtracted from the photopeaks according to their specific regions of interest. A Canaberra Series 95 multi-channel analyzer was used to acquire the data.

6.4 Results: Table 6.1 shows the results of neutron activation analysis for the calcite samples. The data is normalized to the 1.159 MeV γ ray corresponding to calcium.

Table 6.1. Results of neutron activation analysis for three different calcite sample types. The data is normalized to the 1.159 MeV γ corresponding to calcium.[17] Dashes denote that a specific γ ray was not detected.

Energy	Impurity	Swakopmund	Iceland Spar	Gallatin
1.783		472	212	542
1.768		35	19	64
1.755		--	11	--
1.502		18	20	--
1.464		164	67	248
1.371	Mg	--	20	86
1.335		48	30	79
1.296	Ca	187	167	229
1.278		--	--	79
1.176		--	38	--
1.159	Ca	332	332	332
1.128		49	52	--
1.099		46	--	61
1.028		28	26	--
0.912	Y	45	19	54
0.848	Mn	--	--	103
0.727		75	30	99
0.663		74	39	--
0.652		43	--	--
0.610		102	73	238
0.584		--	49	--
0.512	Zn	--	310	--
0.357		--	--	122
0.352		--	69	143

Because of time and software limitations, only emission energies that were characteristic to a type of calcite were analyzed. A γ ray that is emitted by only one or two of the samples is considered to be "characteristic" in reference to a specific sample. The determined impurities are listed on the table next to their emission energies. Zinc was found only in Iceland Spar calcite, and manganese was found only in the Gallatin calcite. Yttrium was observed to be present in all three samples. According to γ ray emission, Iceland Spar calcite contained the greatest variety of impurities and Gallatin calcite contained the least.

6.5 Discussion: Neutron activation data is usually analyzed by a computer, especially to determine which radionuclides correspond to which gamma rays. Different nuclides may emit γ rays of the exact same energy. In order to remove this ambiguity, different emission spectra are acquired at different time intervals from the termination of sample irradiation. The number of counts in the photopeak will follow the exponential decay law[16]:

$$N_2 = N_1 e^{-\lambda \Delta t} \qquad (6.7)$$

where N_2 and N_1 refer to the net counts under the second and first photopeaks, respectively. The time interval between the first and second counts is Δt. Thus, by knowing the decay constant of the isotopes, one may effectively remove the γ ray ambiguities. Computer software which utilizes this method of interpreting emission spectra exists, however none of it is on hand at USNA. Performing this method without a computer is very tedious work indeed. This factor is one of the primary reasons why all of the emission energies have not been determined. Another important factor that must be taken into account when analyzing the emission spectra

of the calcites is the branching ratio and cross section of the isotope decays. One isotope will commonly exhibit a number of γ ray emissions. Many of the emissions will be observed simultaneously for the same isotope. So as not to associate them with another isotope, the ratio of the number of counts for the two decay energies of the same isotope must be compared to the ratio of their cross sections (as corrected by the γ yield). If the two ratios are of the same order, then both emissions are caused by the same element. Calcium is an excellent example of this. It exhibits two γ ray emissions at 1.296 and 1.159 MeV. For Swakopmund calcite, the ratio of the 1.159 MeV γ ray to the 1.296 γ ray is on the order of 1.8. The ratio of the cross sections corrected by the γ yield for those decays is on the order of 1.9. Hence, conclusive evidence exists linking both emissions to the radioactive calcium isotope.

One final consideration to take into account is that some isotopes are simply not prone to activation with 14.3 MeV neutrons. Two such elements are carbon and oxygen. Although there is one carbon atom and three oxygen atoms for every one calcium atom which exists in the crystal lattice, none of their decay energies are seen in Table 6.1. The same holds true for copper and nickel.

The neutron activation data did confirm some of the results of both atomic absorption and X-ray fluorescence. For example, both neutron activation analysis and X-ray fluorescence showed the presence of yttrium in all three samples. Additionally, just as in X-ray fluorescence, zinc and manganese were observed in Iceland Spar and Swakopmund calcite, respectively via neutron activation analysis.

6.6 Conclusion: Neutron activation analysis has added extra confirmation to a significant portion of the results of both X-ray

fluorescence and atomic absorption. Yttrium impurities were observed in all three samples while manganese and zinc were found only in Gallatin and Swakopmund materials, respectively. Of the three determinative methods employed, the most experimental reliability is associated with neutron activation. Because of the lack of special software needed for data analysis, many possible results of the activation data were not determined.

7. FOURIER TRANSFORM INFRARED SPECTROSCOPY:

7.1 Introduction: The infrared region of the electromagnetic spectrum has wavelengths ranging from 0.75-500 μm. Infrared spectroscopy is a valuable probe in determining structural data. In general, infrared spectroscopy is built upon four postulates: 1) substances exhibit characteristic group frequencies in the infrared region; 2) the absorption spectrum of a given substance is generally specific for that and only that substance; 3) the absorption spectra of mixtures are generally additive, i.e., the sum of the individual spectra of the components; and 4) the intensity of an absorption band is related to the concentration of the substance that absorbs the incident radiation.[19] "Fourier transform" refers to a specific technique used in infrared analysis to circumvent the inability of infrared detectors to accurately measure both the frequency and intensity of infrared radiation.

The decision to perform infrared measurements on the calcite samples was a direct result of what appeared to be quantum tunneling phenomena revealed by dielectric relaxation measurements (see Section 8). Tunneling is often associated with protons. Protons (hydrogen atoms) are primarily found in water molecules and hydroxide ions. Infrared

spectroscopy is one of the best non-destructive methods available for the detection of water within materials.

7.2 Theory:[20] Fourier transform infrared spectroscopy operates on the principle that information obtained from infrared frequencies may be converted to audio frequencies. Audio frequency detectors and electronics are capable of tracking both frequency and intensity parameters. Typical FT-IR spectrometers consist of three components: a source, a Michelson interferometer, and a detector.

The Michelson interferometer is composed of a beam splitter, a fixed mirror, and a moving mirror. Collimated radiation from the source is split into two beams of roughly equal energy. One beam is directed to the fixed mirror while the other is directed to the moving mirror. Both beams reflect from the mirrors and recombine at the beam splitter. Depending on the position of the moving mirror, the beams will interfere either constructively or destructively. This resultant beam is then passed through the sample on its way to the detector resulting in an interference pattern that is a modulated cosine wave. The frequency of the modulated wave is determined by the velocity of the moving mirror. Mathematically speaking, the Fourier transform of a single frequency is a cosine wave.

Thus, the interferometer encodes the initial frequencies into a form the detector can monitor with time. This is accomplished by optically taking the Fourier transform of the incoming signal. An inverse Fourier transformation is then performed to convert the time domain to the desired frequency domain for the final presentation of the infrared spectrum.

7.3 Experiment: A Nicolet Model 740 Fourier Transform - Infrared Spectrometer was used to acquire plots of absorbance versus wavelength for all three of the calcite samples using the potassium-bromide pellet

method. This method entails grinding the samples into a powder. Potassium bromide was added, and the mixture was evacuated in a die and pressed into a pellet by applying a pressure of 15 tons per square inch for 10 minutes. Scanning was performed in the near infrared region over wavenumbers ranging from 4000-500 cm^{-1}.

7.4 Results: Six infrared absorption bands were observed in all three calcite samples. These bands appear as peaks on plots of absorbance versus wavenumber, such as the one shown in Figure 7.1 for a potassium bromide pellet containing Iceland Spar calcite. The bands appearing at 713 cm^{-1}, 873 cm^{-1}, and 1417 cm^{-1} are all associated with the carbonate anion that makes up the crystal lattice of calcite. The absorptions are correlated to the carbonate ion's asymmetric bending mode, out-of-plane bending mode, and asymmetric stretching mode, respectively.[21] The 2513 cm^{-1} band and its associated shoulder peak at 2582 cm^{-1} correspond to the presence of bicarbonate ions. The rather wide hump centered at about 3500 cm^{-1} is commonly attributed to the stretching mode of the hydroxyl ion.[22] Additionally, other minor bands were observed at 1800 cm^{-1}, 2274 cm^{-1}, and 2282 in Iceland Spar calcite. Their identity has not yet been determined. Mid-infrared spectra of potassium bromide pellets containing the other two samples were found to be quite similar to that of Iceland Spar calcite.

In order to quantify the above absorptions bands, the area under each of the peaks was integrated via Nicolet Systems software. The strength of the peak is directly proportional to the concentration of infrared-absorbing species present in the crystal. Ratios of each band were then calculated

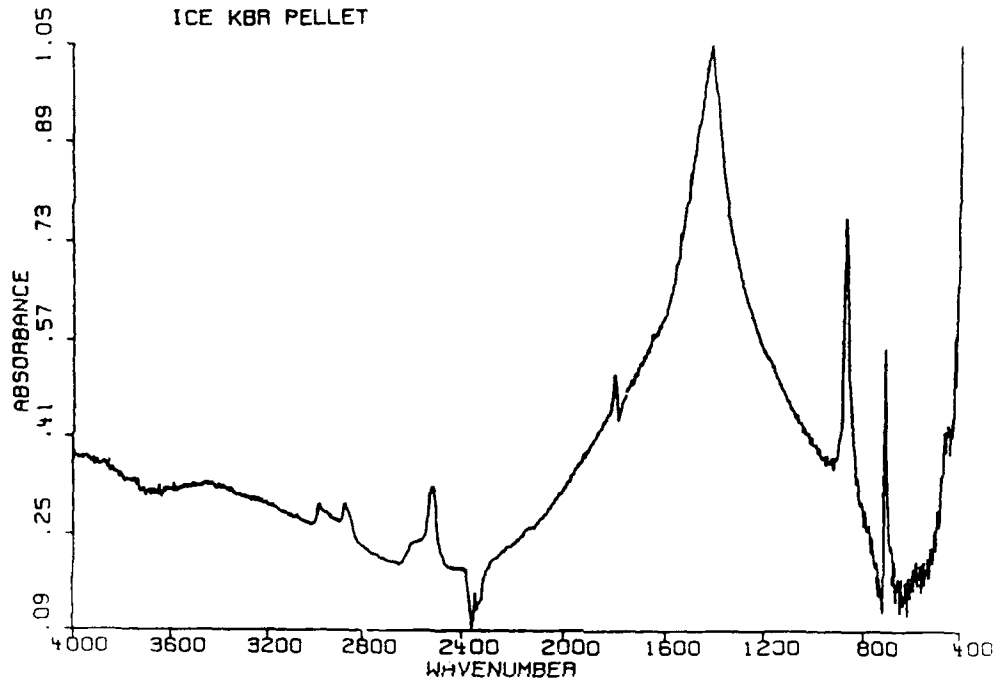

Figure 7.1. Absorbance versus wavenumber (cm^{-1}) resulting from a mid-infrared scan of a potassium bromide pellet containing Iceland Spar Calcite. Absorption bands appear as peaks.

Table 7.1. Relative peak ratios of hydroxyl and bicarbonate ions referenced to the characteristic carbonate band appearing at 713 cm^{-1}.

Sample	Hydroxyl Ion	Bicarbonate Ion
Iceland Spar	0.980	1.719
Gallatin	0.967	1.838
Swakopmund	0.474	1.380

with reference to the characteristic band of carbonate occurring at 713 cm^{-1}. The results for hydroxyl and bicarbonate ions are given in Table 7.1. The table clearly demonstrates that there are more hydroxyl ions and more bicarbonate ions in the Iceland Spar and Gallatin samples than there are in the Swakopmund sample. Additionally, the ratios of each absorption band are roughly on the same order of magnitude in both the Gallatin and Iceland Spar samples.

7.5 Discussion: Although the hydroxyl concentrations appear to be more consistent than those for the bicarbonate ions, certain factors still must be taken into account. The most significant factor affecting hydroxyl impurities is the environment. Where and under what conditions a type calcite is formed will have a profound effect upon its hydroxyl concentration. If it forms in a rather moisture rich environment, then that sample will exhibit a much greater hydroxyl ion concentration than one which was formed in drier surroundings.

Even though the environment does not have such a profound effect upon the bicarbonate ion concentrations, the data regarding those concentrations is considered to be slightly less conclusive than that of the hydroxyl ion. This is primarily attributed to the variations which exist from sample to sample. Notice they are less consistent than the variations

observed with regard to the hydroxyl ion.

Although not shown in the results, the intensity ratio of the 713 cm^{-1} band to the 870 cm^{-1} band was almost precisely the same in all three samples. Because both of these absorption bands are internal standards of calcite, it was assumed that the peak ratio method of quantitative analysis was a valid method of comparison.

7.6 Conclusion: The Gallatin and Iceland Spar samples have almost the same concentration of both hydroxyl and bicarbonate ions. The concentration of the same ions is significantly less in Swakopmund calcite. These findings will be very significant in terms of identifying low temperature relaxations. Typically such relaxations are caused by protons. Protons are found in both types of ions discussed. If these ions are responsible for an observed defect, the measured parameters of that defect should be roughly equal in Gallatin and Iceland Spar calcite and significantly less in Swakopmund calcite.

8. DIELECTRIC RELAXATION SPECTROSCOPY:

8.1 Introduction: The study of dielectric properties is one of the most practical and effective ways to gain an insight into the nature of the internal field that exists between the atoms in a solid. The value of room temperature conductivity not only serves as a general measure of the purity of the solid, but it doubles as an indicator of the concentration of defects in that solid. Dielectric properties additionally aid in understanding the mechanism of electrical conduction.[23] Dielectric loss often arises when defects residing in a crystal lattice have a lower point symmetry than that of the crystal itself. Because the defects usually possess several

crystallographically equivalent orientations, they are capable of preferential reorientation in the presence of an electric field.[24] Many materials, including calcite, will exhibit different dielectric properties when they are examined along different orientations.

8.2 Theory:[25] Relaxation is defined as the delayed response to a changing stimulus in a linear system in which the response and the stimulus are proportional to one another when that system is in equilibrium. In the case of dielectric relaxation, the stimulus is an alternating electric field and the response is a polarization. The relaxation of the polarization is brought about by the thermal motion of the affected atoms. Typically the structural processes involved in dielectric relaxation are difficult problems in statistical thermodynamics. However, the mechanism in calcite may be visualized as involving dipoles of molecular size whose orientations (or magnitudes) fluctuate spontaneously, in thermal motion.[25]

The Debye equations for the dielectric constants form the mathematical basis for the study of dielectric relaxation. They may be derived by contemplating some fundamental electrostatic principles. Consider a capacitor filled with a dielectric material. The charge Q on the capacitor is related to the voltage V across it by:

$$Q = \varepsilon C_o V \qquad (8.1)$$

where C_o is a geometrical factor and ε is a constant with respect to time. A dielectric constant of $\varepsilon > 1$ implies that charge displacements occur within the dielectric. Such responses always need time to occur. In other words, the delayed response of the matter between the plates of the capacitor is due to the procedure by which it causes an increase of capacitance. Thus, a

capacitor with a dielectric will behave like an RC circuit. Because the same differential equations apply to the real capacitor as well as the analog, the dielectric constant ε (t) may be treated as a complex quantity analogous to impedance.[25]

To mathematically arrive at the Debye equations, it is advantageous to work in terms of charge densities and fields. Neglecting edge effects, the electric field E of a parallel plate capacitor has the magnitude:

$$E = \frac{V}{d} \qquad (8.2)$$

where d is the distance between the plates and V is their potential difference. The charge density may be defined as:

$$\sigma = \frac{Q}{A} \qquad (8.3)$$

in which A is the area. The charge density and the electric field are related by:

$$E = 4\pi\sigma_o \qquad (8.4)$$

where σ_o is the charge density for the capacitor in a vacuum. The presence of a dielectric material will increase the charge storage capability of the capacitor (and hence increase the capacitance) so that the final charge density will be:

$$\sigma = \varepsilon_s\sigma_o \qquad (8.5)$$

in which ε_s represents the static dielectric constant. Positive and negative charges in the dielectric material will be displaced slightly from their

normal positions. This polarization will couple with the external field to hold a total charge Q on the plates of the capacitor. It now becomes convenient to introduce a field quantity D defined such that:

$$D = 4\pi\sigma \tag{8.6}$$

where σ is the total charge density resulting from both the action of the external field and the polarization. The polarization P may be defined as the charge density held on the plates by the internal displacement of charges:

$$\sigma_o + P = \sigma \tag{8.7}$$

Manipulating equations (8.4), (8.5), (8.6), and (8.7) gives:

$$E + 4\pi P = D \tag{8.8}$$

while equation (8.5) leads to the result:

$$D = \varepsilon_S E \tag{8.9}$$

This makes it possible to define the static dielectric constant in terms of the polarization:

$$\varepsilon_s - 1 = \frac{4\pi P_s}{E} \tag{8.10}$$

where P_s denotes the static value. In the whole of the capacitor, the implied dipole moment of the dielectric will be:

$$M_s = P_s A d \tag{8.11}$$

implying that P_S represents a dipole moment per unit volume.[25]

Up to this point, it has been assumed that P_s and E were in equilibrium. When E changes with time, P will differ from $P_s(E)$ at any given moment. Because P approaches P_s as the system goes to equilibrium, a differential equation may be assumed for P(t). If the speed of the system's approach to equilibrium is taken to be proportional to the distance from equilibrium,then the differential equation is:

$$\tau \frac{dP(t)}{dt} = P_s - P(t) \qquad (8.12)$$

where τ is considered to be constant. However, before integrating, the above equation must be modified since several different mechanisms of polarization normally operate in a dielectric. Two such mechanisms are electronic and optical polarization[25]. Electronic polarization is responsible for the optical refractive index. Due to its essentially negligible response time to changing electric fields (at all frequencies), it will not enter into the above differential equation. Equation (8.10) will become:

$$\varepsilon_s - 1 = \frac{4\pi}{E}(P_D + P_\infty) \qquad (8.13)$$

in which P_∞ denotes the optical polarization and P_D refers to the static "dipolar" polarization. The optical dielectric constant may be defined as[25]:

$$\varepsilon_\infty - 1 = \frac{4\pi P_\infty}{E} = n^2 - 1 \qquad (8.14)$$

n being the refractive index of the dielectric material. Applying an electric field E(t) to the dielectric will cause $P_\infty(E)$ to respond instantaneously

while P_D will respond according to the modified differential equation in (8.12):

$$\tau\frac{dP_D}{dt} + P_D(t) = (\varepsilon_s - \varepsilon_\infty)\frac{E(t)}{4\pi} \qquad (8.15)$$

The right side of the equation is the equilibrium value that corresponds to E(t), assuming that the instantaneous value of E(t) were to be applied for an infinite amount of time. This equation is analogous to the equation for the charge on a capacitor when it is in series with a resistor. In a periodic field, the general solution to such an equation would be:

$$E^*(t) = E_0 e^{i\omega t} \qquad (8.16)$$

In terms of the complex quantity for the dipolar polarization P_D^*, equation (8.15) becomes:

$$P_D^*(t) = Ke^{-(1/\tau)} + \frac{1}{4\pi}\frac{\varepsilon_s - \varepsilon_\infty}{1 + i\omega\tau}E_0 e^{i\omega t} \qquad (8.17)$$

where K characterizes the initial polarization[25]. The negative exponential will cause the first term to be negligible in comparison with the second term. Thus, a complex dielectric constant may be defined as:

$$\varepsilon^*(\omega) - \varepsilon_\infty = 4\pi\frac{P_D^*(\omega,t)}{E^*(\omega,t)} \qquad (8.18)$$

This is analogous to the complex capacitance of an RC circuit. Separating $\varepsilon^*(\omega)$ into its real and imaginary parts yields:

$$\varepsilon^*(\omega) = \varepsilon'(\omega) - i\varepsilon''(\omega) \qquad (8.19)$$

in which:

$$\varepsilon'(\omega) = \varepsilon_\infty + \frac{\varepsilon_s - \varepsilon_\infty}{1 + \omega^2\tau^2} \qquad (8.20)$$

$$\varepsilon''(\omega) = (\varepsilon_s - \varepsilon_\infty)\frac{\omega\tau}{1 + \omega^2\tau^2} \qquad (8.21)$$

Equations (8.20) and (8.21) are known as the Debye equations.[25] The value for ε'' may be found experimentally by measuring ε' and the loss tangent defined by:

$$\tan\delta = \frac{\varepsilon''(\omega)}{\varepsilon'(\omega)} = \frac{G}{\varepsilon_o\omega}\frac{1}{\varepsilon'(\omega)} \qquad (8.22)$$

where G and ε_o denote the electrical conductivity and the permittivity of free space, respectively. Hence, the loss tangent additionally represents a measure of the ratio for the conduction current relative to the displacement current.[26] In order to determine the value for ε'', the capacitance and the ratio of conductance frequency (G/ω) must be measured.

8.3 Sample Preparation: In order to prepare the calcites for dielectric relaxation measurements, the orientation of the optic axis within the crystal had to be determined. This was done by visually locating one of the two points of three-fold symmetry while the chunk of crystal was lying on a cleavage surface parallel to a rhombohedron face. From this three-fold point of symmetry, the *c* axis runs through the chunk at an angle of 45°36' to the rhombohedron face (as mentioned in Section 2). A wire saw was then used to cut samples of the calcite chunk either parallel or

perpendicular to the *c* axis. The plate-shaped samples were ground to a thickness ranging from 0.70 to 1.50 mm and finished in most cases using 4/0 grit Carborundum polishing paper. The orientation of the *c* axis was checked using cross polaroids and determined to be in error by no more than 3 degrees. Cleaved samples (also under 1.50 mm thick) were prepared in addition to those that were cut and ground. The *c* axis has no specific orientation with respect to the faces of the cleaved samples. Aluminum electrodes were evaporated onto the "cut and ground" and cleaved samples in a "three electrode" and "two electrode" configuration, respectively. The core of the central guarded region for the "three electrode" configuration was 9 mm. Such a configuration is used to prevent any surface conduction that may take place directly between the two electrodes on the sample as a result of fringing field effects.[24]

As an aside, a very interesting phenomenon occurred while the samples were being ground. Recall that the calcium and the carbonate planes are perpendicular to the optic axis. In other words, a vector normal to those planes would be parallel to the *c* axis. Bonding forces are also considered to be weak across those planes. This may explain why the samples were extremely easy to grind when the optic axis ran normal to their face and very difficult to grind when the *c* axis ran parallel to their face. In fact, it took almost five times as long to grind a parallel sample than it would to grind an equal amount of the perpendicular sample. This appears to be logical when one considers that the bonding forces between planes of molecules are considered to be "weak." When the *c* axis was normal to the face of the sample, whole planes of either calcium or carbonate ions were being ground off. When the *c* axis was parallel to the sample face, a tiny bit of every single plane was being ground off

simultaneously. An analogy here can be drawn to a stack of 100 sheets of paper. Let each sheet of paper represent a molecular plane. The stack of paper needs to be reduced to a thickness of about ten sheets. In order to achieve the desired thickness, it would be easier to remove the paper sheet by sheet than it would be to throw the whole stack on a paper cutter and cut all 100 sheets simultaneously bit by little bit.

8.4 Experiment: Complex impedance measurements were carried out using a CGA-82 microprocessor controlled capacitance bridge operating at seventeen audio frequencies ranging from 10 to 10^5 Hz. Temperatures over the range of 4.5 to 380 K were established using a precision Cryogenics CT-14 dewar controlled by a Lake Shore Cryotronics DRC-82 temperature controller utilizing a silicon diode. The data taken was transformed via computer to the complex dielectric constant $\varepsilon^*=\varepsilon'-i\varepsilon''$ using techniques described elsewhere.[27] The computer programs employed for data reduction were written in BASIC. Eight experimental runs were performed. Run 1 was conducted with the cleaved samples, and Run 2 with the samples that were cut perpendicular and parallel to the *c* axis. Runs 3, 4, 5, and 6 were performed to confirm the reproducibility of the data taken in runs one and two. Run 7 and Run 8 were performed to check for effects produced by radiative bombardment and for low energy quantum tunneling, respectively.

The resultant values of capacitance and the ratio of conductance divided by angular frequency were transformed to the imaginary part of the dielectric constant (dielectric loss). The values of the real dielectric constant at about 5.5 K were set equal to 8.219 and 7.633, perpendicular and parallel to the *c* axis,respectively. The value for the cleaved samples was set at 7.926.[13]

Figure 8.1. The imaginary part of the dielectric constant versus temperature for various cleaved samples of calcite at a frequency of 10^3 Hz. Straight line segments connect the datum points. The samples are: solid - Swakopmund; short dash - Iceland Spar; dash dot (chain) - Gallatin.

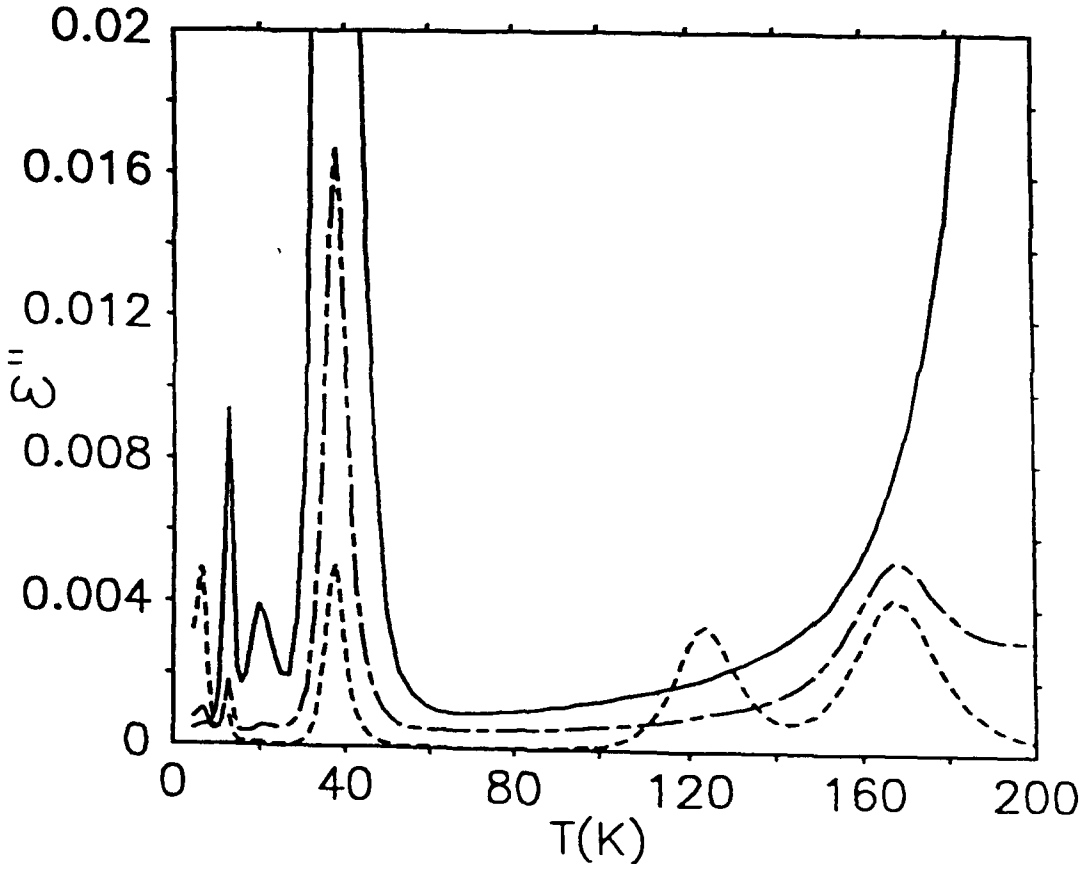

Since corrections for thermal expansion make a small contribution to dielectric loss, it was next assumed that the relative change in the dielectric constant is equal to the relative change in capacitance.[28]

8.5 Results: The results for the imaginary part of the dielectric constant for each type of calcite sample at a frequency of 10^3 Hz and over a temperature range of 4.8-200K are shown in Figure 8.1. The principal relaxations for each material are apparent. The Swakopmund sample (solid line) exhibited three principal relaxations occurring at temperatures of 13K, 21K, and 38K, respectively. The Iceland Spar sample (dashed line) exhibited six principal relaxations at temperatures of 7K, 13K, 38K, 121K, 168K, and 220K. The Gallatin sample (dash-dot line) exhibited six principal relaxations at temperatures of 7K, 13K, 21K, 38K, 168K, and 220K. The 13K and the 38K relaxations were common to all three samples. Both relaxations were more pronounced in the Swakopmund calcite. The 7K, 168K, and 220K relaxations were common to both the Gallatin and Iceland Spar samples. The 21K relaxation was common to only the Swakopmund and Gallatin samples. Table 8.1 shows the principal relaxations and their peak heights for all of the materials. The dielectric loss is assumed to be caused by various trace impurities that were presumably introduced in the natural growth process of the crystals. Note that Swakopmund calcite exhibits the least complicated dielectric spectrum although neutron activation analysis showed that it contains a large number of impurities. This implies that many of the impurities found in Swakopmund calcite do not give rise to dipolar complexes. The reasons behind this behavior will be discussed in the next section.

In order to obtain information concerning the symmetry of the defect sites, measurements were carried out both parallel and perpendicular

to the optic axis on some of the calcites. Figure 8.2 shows the results for the imaginary part of the dielectric constant versus temperature at a frequency of 10^3 Hz for those specific orientations of the optic axis in the Iceland Spar sample. Clearly, the 7K and the 13K relaxations were seen only when the optic axis was oriented

Table 8.1. Peak relaxation values for ε''(max) in Swakopmund, Iceland Spar, and Gallatin Mountain calcite samples at a frequency of 10^3 Hz and various orientations.

Sample (Cut)	7K	13K	21K	38K	121K	168K	220K
ICELAND SPAR							
#1(Cleave)	0.002			0.00017	0.022	0.0044	0.00006
#2(Cleave)	0.002			0.00008	0.001	0.004	0.0002
(⊥)	0.005	0.001				0.00067	
(∥)				0.005	0.0034	0.0042	
GALLATIN MOUNTAIN							
#1(Cleave)	0.00045	0.00055	0.0005	0.0052		0.0018	0.0015
#2(Cleave)	0.0006	0.0014	0.00012	0.016		0.003	0.0002
#3(Cleave)	0.00043	0.00041	0.00005	0.007		Noise	Noise
SWAKOPMUND							
#1(Cleave)		0.0002		0.0047			
#2(Cleave)		0.0037	0.0015	0.051			
#3(Cleave)		0.008	0.003	0.10			
#4(Cleave)		0.004	0.002	0.099			
(⊥)		0.022					
(∥)			0.011	0.4			

perpendicular to the electric field (solid line). When oriented parallel to the field (dashed line), the 38K and the 121K relaxations then became visible while the 7K and 13K relaxations disappeared. The 168K relaxation, on the other hand, is observed both parallel and perpendicular

Figure 8.2. The imaginary part of the dielectric constant versus temperature for Iceland Spar calcite parallel and perpendicular to the optic axis at a frequency of 10^3 Hz. Straight line segments connect the datum points. The samples are: solid - perpendicular to the *c* axis; short dash - parallel to the *c* axis.

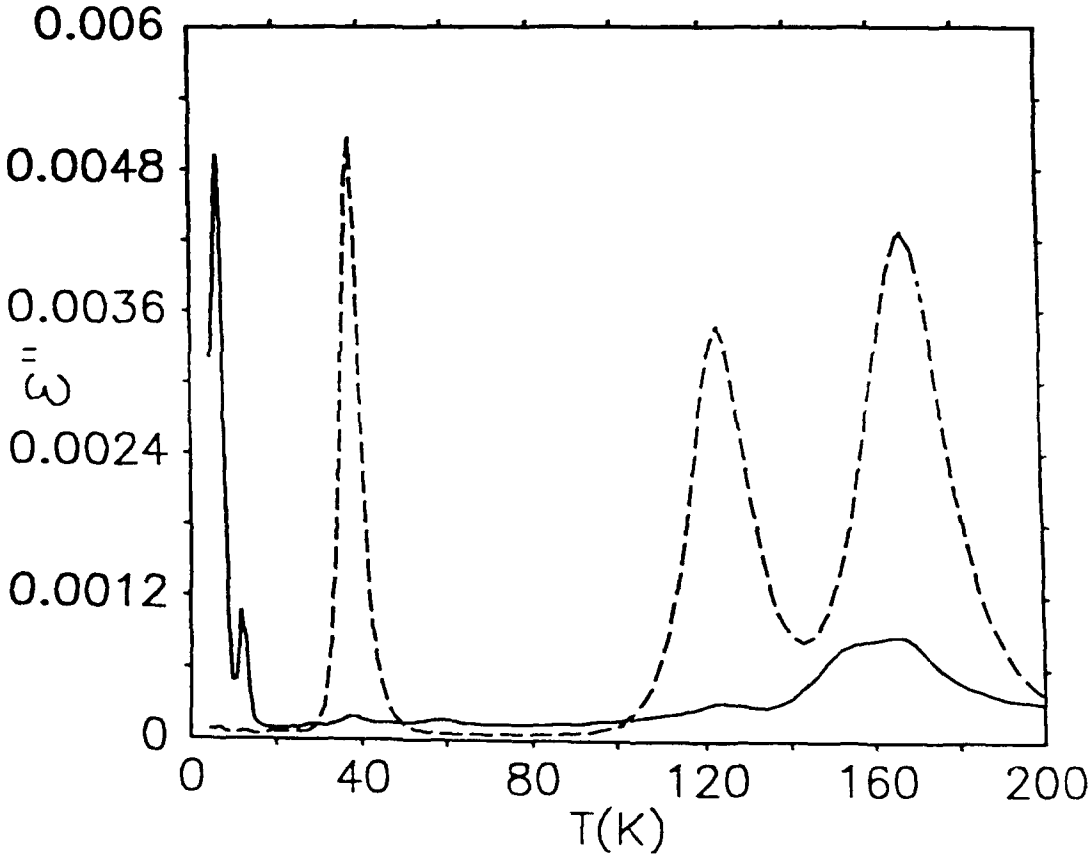

Figure 8.3. The imaginary part of the dielectric constant versus temperature for Swakopmund calcite parallel and perpendicular to the optic axis at a frequency of 10^3 Hz. Straight line segments connect the datum points. The samples are: solid - perpendicular to the *c* axis; short dash - parallel to the *c* axis.

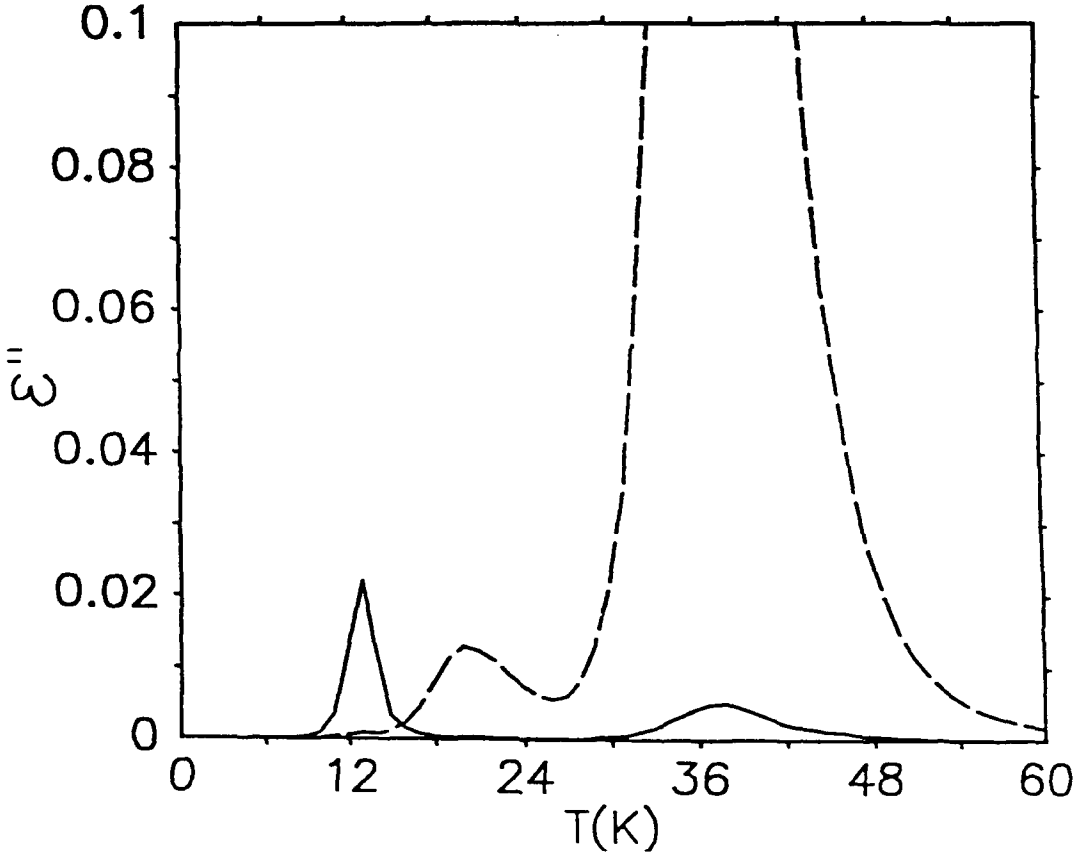

to the optic axis. It is stronger by about a factor of three along the axis. Figure 8.3 is a plot shows the same plot for the Swakopmund calcite. At parallel orientations (dashed line), the 21K and the 38K relaxations are apparent. At perpendicular orientations (solid line) only the 13K peak was seen. Traces of the 38K peak are also observed in this orientation to the *c* axis, but the strength was at least 50 times weaker than in the parallel orientation. Possibly, the appearance of the 38K relaxation when measured perpendicular to the field is caused by uncertainty in the actual orientation of about a few degrees of arc. Figures 8.2 and 8.3 clearly show that the value of ε'' depends greatly upon the orientation of the optic axis. In summary, the 21K, 38K, and the 121K relaxations are observed in parallel *c* axis orientations. The 7K and the 13K, relaxations are observed in perpendicular *c* axis orientations. The 168K relaxation is the only one which is observed in both directions of axial orientation.

In order to evaluate each of the relaxations quantitatively, a characteristic relaxation time, τ, was determined for each relaxation observed. This was accomplished by constructing plots of ε'' versus the applied frequency for a specific temperature. Figure 8.4 shows a typical data set for Swakopmund calcite at temperatures of 35.0K (triangles) and 36.8K (squares). The optic axis was in a parallel orientation. The relaxation time is defined to be the reciprocal of the peak position, i.e. $\omega_{max}\tau = 1$. Take note of how the peak position depends on temperature. For one characteristic relaxation, there will be numerous relaxation times depending upon the temperature at which the data was acquired. Best values of ω_{max} were obtained by fitting the empirical Cole-Cole expression[29]:

Figure 8.4. The imaginary part of the dielectric constant versus the log of the frequency (Hz) at two temperatures for Swakopmund calcite cut to have a parallel orientation of the optic axis. Solid lines are the best fit Cole-Cole curves of Equation 8.23. The temperatures are: triangle - 35.0K; square - 36.8K.

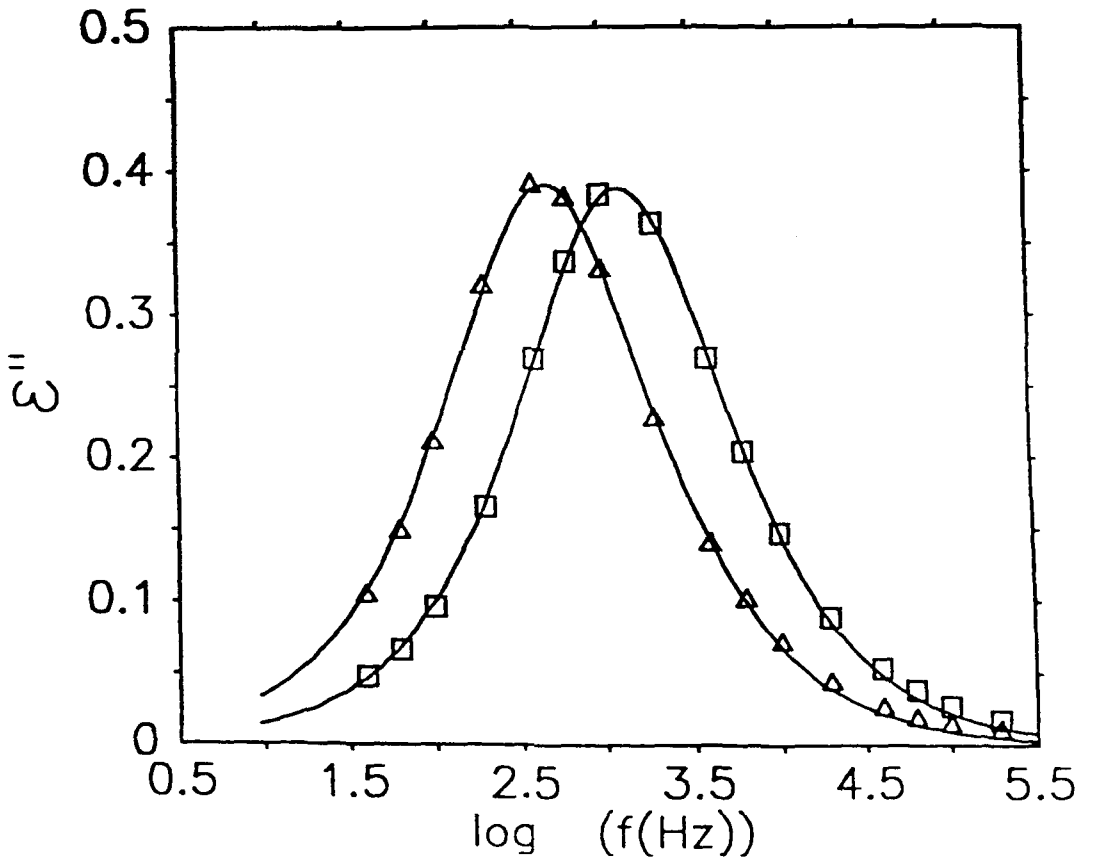

$$\varepsilon'' = \frac{(\varepsilon'_L - \varepsilon'_H)\cos(\alpha\pi/2)}{2\{\cosh[(1-\alpha)x] + \sin(\alpha\pi/2)\}} \qquad (8.23)$$

to the data. These fits are the smooth curves in Figure 8.4. α is the constant Cole-Cole parameter and $x = \ln(\omega\tau)$. ε'_L and ε'_H are the 'low' and 'high' frequency limits of the dielectric constant where 'low' and 'high' mean relative to the effects of the relaxation only. The best fit results showed that[30]:

$$\varepsilon'_L - \varepsilon'_H = \frac{A}{T} \qquad (8.24)$$

where A is known as the dipole strength. The value of A is given by:

$$A = \frac{Np^2}{3\varepsilon_o k_b} \qquad (8.25)$$

where N is the concentration of the dipoles, ε_o is the permittivity of free space, and p is the dipole moment. It is interesting to note just how sensitive dielectric relaxation spectroscopy is. For a typical weak peak, A = 0.005, and the concentration of the dipoles is on the order of 50 parts per billion ($5 \times 10^{-6}\%$)[31].

Finally, plots of the relaxation time versus the reciprocal of temperature were constructed in order to check for Arrhenius behavior, as described by the equation:

$$\ln(\tau) = E / k_b T + \ln(\tau_o) \qquad (8.26)$$

Figure 8.5. The natural log of the relaxation time versus the reciprocal of temperature of the 38K relaxation in Swakopmund, Iceland Spar, and Gallatin calcites. The solid line in the figure is the least squares best fit line (Arrhenius expression: Equation 8.26) to the data for the Iceland Spar calcite. The samples are: triangle - Swakopmund parallel to the *c* axis; x - Gallatin cleave; square - Iceland Spar parallel to the *c* axis.

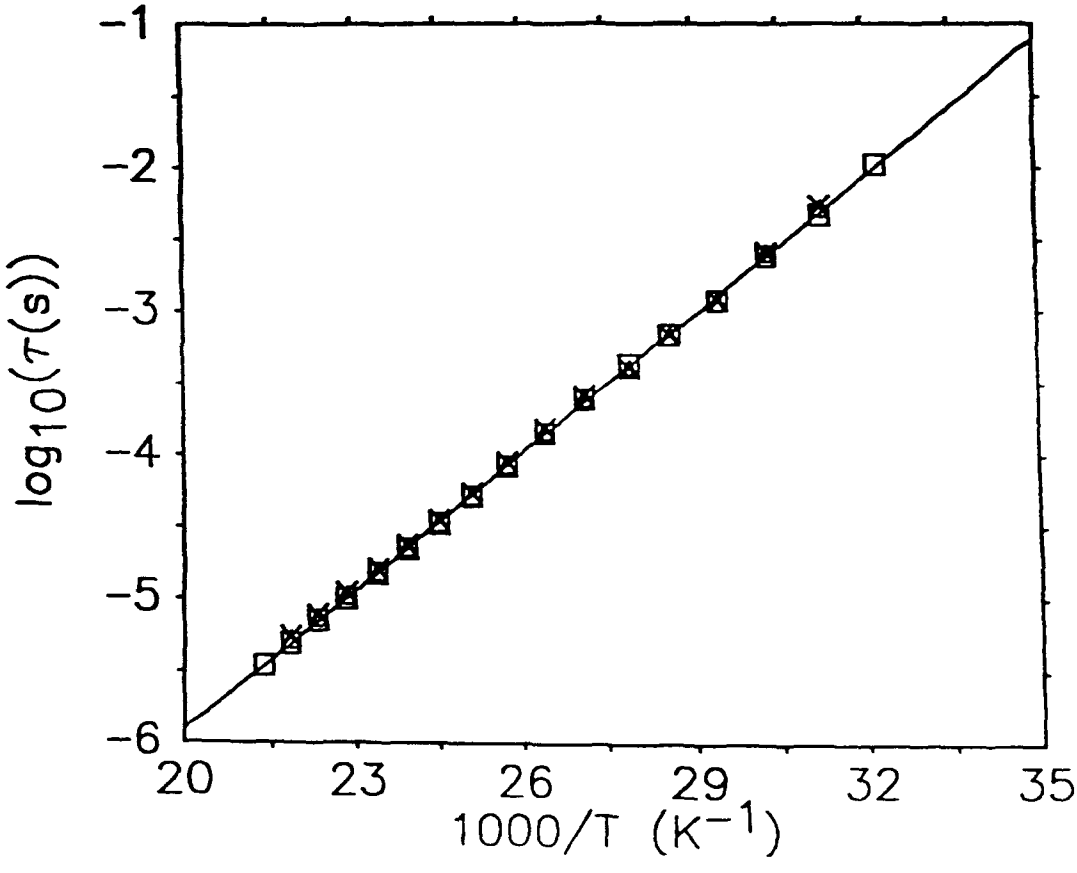

Figure 8.5 shows the Arrhenius plot for the 38K relaxation appearing in all three samples. E and τ_o are constants known as the activation enthalpy and the reciprocal frequency factor, respectively. Boltzmann's constant is denoted by k_b. Equation 8.26 was least squares best fit to the data. All of the relaxations behave in a similar Arrhenius manner except the one observed at 7K. It is clear from Figure 8.5 that the 38K relaxation is caused by exactly the same defect complex in all three samples. All of the samples which demonstrate Arrhenius behavior possess values for $\log_{10}(\tau_o)$ that are on the order of -12. This value is typical of the reciprocal of a lattice vibrational frequency.

The Arrhenius plot for the 7K relaxation in Iceland Spar and Gallatin calcite is non-linear, as shown by Figure 8.6. The curve has both a linear and exponential region and is characteristic of some type of quantum tunneling phenomena. There will be a linear dependence of τ^{-1} on T in the lowest temperature range and a power-law increase at higher temperatures:

$$\tau^{-1} = AT + BT^n \qquad (8.27)$$

where n should fall between 4-7 depending on how the very detailed theoretical aspects of such phenomena are interpreted[32,33,34,35]. The linear and power law dependence are characteristic of single-phonon and multiphonon processes, respectively. In the multiphonon region, the "exponential Arrhenius" dependence may alternatively take the form of[24]:

$$\frac{1}{\tau} = B\,T + \frac{1}{\tau_O} \exp\left(\frac{-E}{k_b\,T}\right) \qquad (8.28)$$

Figure 8.6. The natural log of the relaxation time versus the reciprocal of temperature showing non-Arrhenius behavior (quantum tunneling) in both the Gallatin and Iceland Spar calcite. The solid lines are the best fit theory based on Equation 8.28. The samples are: square - Iceland Spar; triangle - Gallatin.

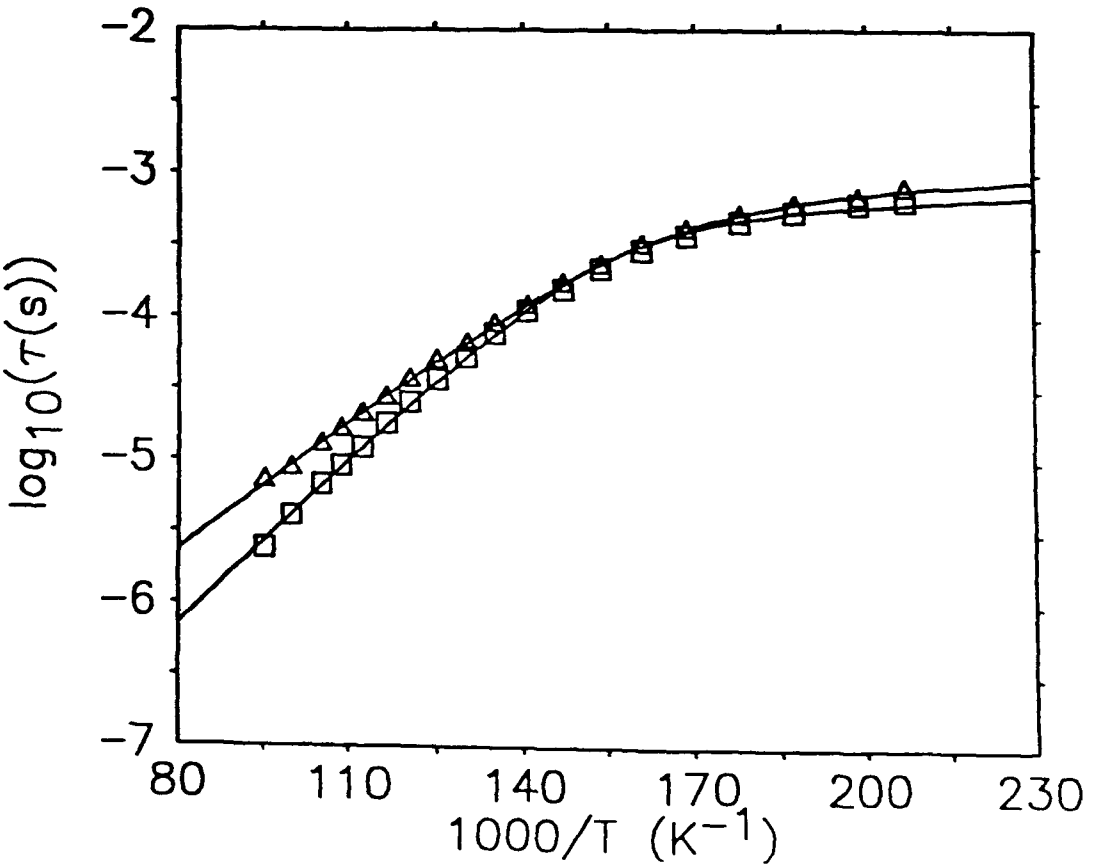

from which the best fit parameters of Equations 8.23 and 8.26 can still be determined. The values of $\log_{10}(\tau_o)$ are -9.2 and -8.0 for Iceland Spar and Gallatin calcite, respectively. All of the best fit quantitative parameters for both Arrhenius and non-Arrhenius behavior are listed in Table 8.2. The estimated errors in E and $\log_{10}(\tau_o)$ are about 1%.

Table 8.2. Relaxation parameters for the principal relaxations observed in Swakopmund, Iceland Spar, and Gallatin Mt. calcite. Parallel and perpendicular c axis orientations are denoted by ∥ and ⊥, respectively.

Sample(Cut)	T(K)	E(eV)	$\log_{10}(\tau_o)$ (s)	A(K)	α	B(1/K-S)
Gallatin(cleave)	7	0.0059	- 8.01	0.0047	0.09	253
IcelandSpar(⊥)	7	0.0076	- 9.20	0.0282	0.08	328
Gallatin(cleave)	12	0.0237	- 12.02	0.034	0.07	-
Swakopmund (∥)	38	0.0631	- 12.26	37.0	0.13	-
Gallatin(cleave)	38	0.0628	- 12.20	1.39	0.08	-
IcelandSpar(∥)	38	0.0634	- 12.29	0.40	0.03	-
IcelandSpar(∥)	121	0.2201	- 12.77	0.87	0.05	-
IcelandSpar(∥)	168	0.2907	- 12.53	1.31	0.04	-
Gallatin(cleave)	168	0.2975	- 12.72	1.13	0.02	-

8.6 Discussion: As shown by the figures and the results in the tables, the existence of a particular sequence of peaks seems to be characteristic of the origin of the sample. The Arrhenius plot of Figure 8.5 is a very good indication of how well defined the relaxations actually are. Clearly, data for a particular peak in different samples are virtually indistinguishable. Therefore, the activation enthalpy and the reciprocal frequency factor are unique for a given relaxation process. The rather significant variation of the peak height from sample to sample additionally implies that the

concentration of defects appreciably varies from sample to sample. However, this should be expected since the calcites are naturally occurring materials.

As mentioned previously, the 7K relaxation exhibits non-Arrhenius behavior that is characteristic of quantum tunneling. Impurity movement is seen perpendicular to the optic axis which implies that the dipole is moving among equivalent sites which are located within a plane of cations or anions. Such data suggests that this reorientation may be due to the motion of a very small charged particle such as a proton.

Fourier transform infrared spectroscopy (Section 7) revealed two possible origins for this relaxation. First, it was observed that Iceland Spar and Gallatin calcites contained about the same amount of hydroxyl ions (OH^-) via the absorption which was seen at 2.8 μm (3500 cm^{-1}). Although the same absorption was seen in the Swakopmund calcite, the concentration of the hydroxyl ions was significantly less. Second, another absorption at 2500 cm^{-1} showed similar concentrations in the Iceland Spar and Gallatin calcites. This particular absorption is characteristic of the bicarbonate ion, $(HCO_3)^{-2}$. Previous studies have justified the existence of bicarbonate ions in naturally occurring calcite.[36] Again, its concentration was significantly less in the Swakopmund sample.

Because the 7K relaxation is not observed in the Swakopmund sample, the cause of this relaxation is attributed to protons or electrons from either the hydroxyl or bicarbonate ions. Presently, it is not understood how the hydroxyl ions would be incorporated into the $(CO_3)^{-2}$ planes or how the motion of the protons would be restricted only to that plane. On the other hand, it is more intellectually satisfying to visualize bicarbonate ions existing in the plane of the carbonate anions. Such a

defect complex simply requires the addition of a proton to one of those anions. In this case, reorientation would occur when that proton jumped between the carbonate ions. Due to the simplicity of this bicarbonate model, it is the preferred one for the 7K relaxation.

The 38K relaxation is observed in all three of the samples. Neutron activation analysis and X-ray fluorescence have shown that there are several impurities common to all three materials. However, not all of these impurities are likely to give rise to a dipolar defect. For example, strontium is observed in all of the samples. In order for strontium to give rise to a dipolar defect, it would have to substitutionally replace calcium. With an ionic radius of 1.32 Å, this would be impossible.[37] More than likely, only small isovalent impurities will give rise to dipolar defects. Such defects usually arise through charge compensation when an oppositely charged entity is incorporated into the crystal lattice to form a classical dipole.

Of all the impurities that are common to every sample, yttrium is the candidate most likely to form a defect. It is small enough be incorporated into the lattice either substitutionally or interstitially. Further evidence associating it with the 38K relaxation exists. Its photopeak strength as determined via activation analysis is correlated to the strength of the 38K relaxation. This relaxation is the weakest in Iceland Spar calcite. Consequently, yttrium's weakest photopeak is also observed in the Iceland Spar calcite.

Unlike the 7K relaxation, the 38K relaxation implies that impurity movement occurs parallel to the optic axis. Thus, as this dipole moves, it will jump over ionic planes instead of jumping within one. The defect complex for this relaxation has been postulated on the basis of previous

electron spin resonance studies which have concluded that interstitial yttrium has an equal probability of being displaced above or below the carbonate anion plane.[38] It is proposed that Y^{+3} sits interstitially in the lattice and is stabilized by a $(CO_3)^{-3}$ radical that substitutionally replaces a $(CO_3)^{-2}$ anion. As the dipole flips under the influence of the electric field, the yttrium will jump over the carbonate plane. Additional studies have shown that large numbers of yttrium stabilized defects do exist in unirradiated, natural calcite.[9] Additional experiments will be performed to determine if the 38K relaxation is correlated to a 500K radiation induced thermoluminescence peak that is exhibited by other types of blue calcite similar to the Swakopmund sample[39]. The presence of such a correlation would imply that dielectric spectroscopy could be used to evaluate radiation effects and hence be of great interest in dating inorganic materials.

Like the 38K relaxation, the 13K relaxation also appears in all of the samples. Although it is observed parallel to the optic axis instead of perpendicular to it, this relaxation additionally appears to be caused by the presence of Y^{+3} - $(CO_3)^{-3}$ pairs. In this relaxation however, the yttrium becomes the substitutional impurity which stabilizes the interstitial carbonate radical. The $(CO_3)^{-3}$ radicals are formed when an electron jumps among equivalent sites within the carbonate plane in conjunction with a $(CO_3)^{-2}$ ion. Such movement would explain the low activation enthalpy (0.024 eV) of this relaxation. More evidence supporting this defect becomes apparent when the low temperature end of the 13K relaxation is examined. Indications of the onset of quantum tunnelling exist that are consistent with the characteristics of electron motion at low temperatures.

Supporting evidence for defect complexes associated with the 21K,

121K, 168K, and 220K relaxations is not as strong as it was for the last three cases. The 121K relaxation was only observed in the Iceland Spar calcite. It occurred parallel to the optic axis. Neutron activation analysis revealed four impurities unique to that sample. X-ray fluorescence only confirmed the presence of zinc though. Based strictly on ionic size considerations, zinc can be postulated to substitutionally replace the calcium cation providing that equivalent positions exist off center towards the carbonate planes. Whether or not such a mechanism exists in calcite has not yet been determined.

The most likely impurity associated with the 168K relaxation is magnesium because it is the only impurity common to both the Iceland Spar and Gallatin samples. Ionic movement is observed both perpendicular and parallel to the optic axis in this case. Although two equivalent positions exist near the calcium ions, it is not clear how magnesium could give rise to the relaxation since there appears to be no need for charge compensation. Another possible mechanism for this relaxation would be an unidentified substitutional-interstitial complex similar to that of the 13K and 38K relaxations.

The mechanisms associated with the 21K peak in Swakopmund calcite and the 220K peak in Gallatin and Iceland Spar calcite are presently unclear. Although neutron activation has revealed the presence of one impurity which is unique to Swakopmund calcite, its identity could not be determined. Information regarding the 220K relaxation is so sparse that speculations as to its origin will not even be considered.

8.7 Conclusion: The defect complexes for three of the seven principal relaxations have been postulated with a high degree of certainty. The tunneling of protons associated with bicarbonate ions is proposed for

the 7K relaxation. Both the 13K and 38K relaxations appear to be caused by the presence of Y^{+3}-$(CO_3)^{-3}$ substitutional-interstitial impurity pairs. Yttrium is interstitial and substitutional in regard to the 38K and 13K relaxations, respectively. The 121K and 168K relaxations appear to be associated with zinc and magnesium, respectively. The origins of the 21K and the 220K peak are both unclear at the present time. The postulated defect complexes are consistent with results of Fourier transform infrared spectroscopy, neutron activation analysis, atomic absorption, and X-ray fluorescence.

9. RADIATIVE BOMBARDMENT:

9.1 Introduction: This particular experiment was prompted by both the results of various thermoluminescence studies and the results of optical absorption. Because no significant absorbance bands were seen in either the Swakopmund or the Iceland Spar calcite, it was assumed that the color mechanisms did not depend on impurity content [recall in Section 3.4 that experimental evidence has been found linking manganese impurities to the yellowish hue in Gallatin calcite[10]].

Although the color mechanisms in calcite are still not completely understood, they appear to be associated with various thermoluminescence phenomena. Thermoluminescence refers to a process in which stored energy in a material is released as light when the material is heated. Often, this energy is imparted to the material by damaging it in some way, such as through ion bombardment. Luminescence usually occurs when there is an effective movement of charge from a trapping center to a recombination site of some type.[40]

It has been shown experimentally that blue and violet colors may be induced in some calcites by irradiation after compression.[39] Those colors then disappeared with accompanying thermoluminescence. The appearance of those colors was thought to be correlated to, but not caused by, the presence of iron or manganese atoms in solid solution.[41] However, results of another experiment have shown that upon irradiation by X-rays, calcites with the same concentrations of iron, manganese, magnesium, strontium, copper, and barium exhibited very different absorption bands after undergoing thermoluminescence.[39] It has additionally been concluded that the decay of thermoluminescent light output and dielectric loss of calcite crystals after irradiation are intimately connected.[42]

Due to the various opinions on how the color mechanisms of calcite are influenced by radiation, the decision was made to irradiate our three calcite samples with the hope of producing some radiation induced defects. Should such defects be induced, they may have an effect on the dielectric spectrum of calcites since radiation, thermoluminescence, and dielectric relaxation all appear to be inter-related.

9.2 Experiment: Four Swakopmund, three Iceland Spar, and three Gallatin calcite samples were irradiated by γ rays from a ^{60}Co source at The Naval Research Laboratory in Washington, D.C. Dielectric relaxation spectroscopy had been performed on each sample prior to bombardment. The samples were placed in an aluminum container above a submerged ^{60}Co source. The calcites were irradiated for one hour receiving a total dose of approximately 4×10^6 Rads using Rads(silicon) as a reference for the calculation. After irradiation, the samples were loaded into a capacitance bridge and stored under vacuum at 77K until dielectric readings were acquired.

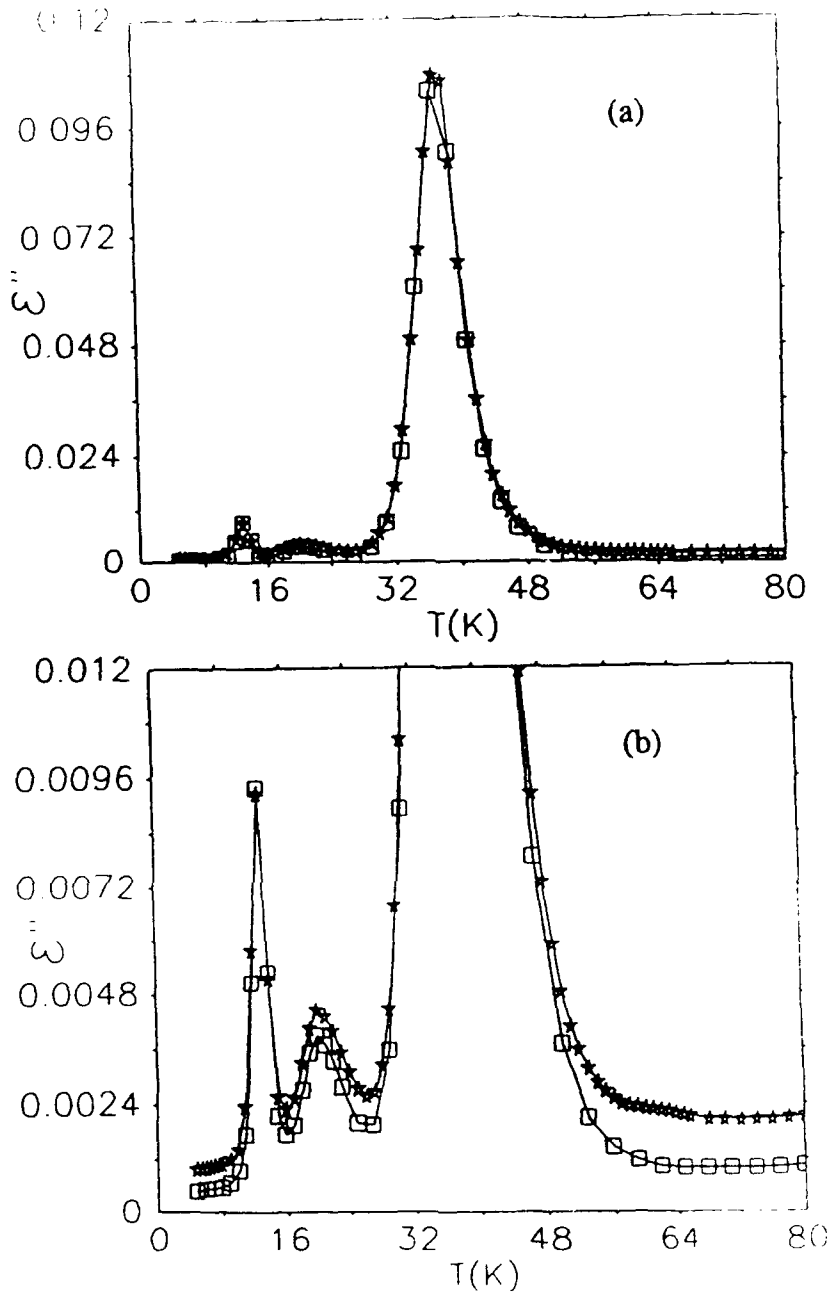

Figure 9.1. The imaginary part of the dielectric constant versus temperature for a Swakopmund cleave irradiated with gamma rays. The squares and stars represent data which was taken before and after irradiation respectively. (b) is the same plot as (a) except that it is shown on a scale 10 times smaller than that of (a). Straight lines connect the datum points.

9.3 Results: The imaginary part of the dielectric constant versus temperature may be seen in Figure 9.1 (a) for a Swakopmund cleave. Both "before" and "after" plots have been superimposed on the same set of axes with squares representing the data before irradiation and the stars representing the data after irradiation. As exhibited in (a), there has been essentially no change in the characteristic dielectric signature of Swakopmund calcite after it had been bombarded with γ rays. Figure 9.1 (b) is the same plot as (a) except that it is shown on a scale 10 times smaller than (a). This was done to emphasize how similar the two signatures really are. Aside from the irradiated data having a slightly higher background than the non-irradiated data, the agreement between the two is almost exact. Both the Iceland Spar and Gallatin samples exhibited exactly the same behavior as the Swakopmund sample did. There was no significant change detected in dielectric signature of the calcites after irradiation.

9.4 Discussion: No appreciable change in the dielectric signatures of the calcites was exhibited as a result of γ ray bombardment. However, this does not imply that no defects were induced by the radiation. In fact, some type of transient defects were introduced into both the Gallatin and the Swakopmund calcite because the colors of those samples changed. The Swakopmund sample became a much darker blue, and the Gallatin sample turned a milky brown that was almost totally opaque. Although Iceland Spar exhibited no noticeable change, change in the other samples occurred on such a macroscopic scale that it was visible to the naked eye.

Why did these defects not appear in the dielectric signature that was acquired after irradiation? There are three possible reasons. First of all, the induced defects may have been highly unstable and hence very transient. The drive from NRL to USNA is approximately one hour. The

defects could have disappeared by that time. Along similar lines, the samples were not cooled down to 77K until approximately four hours after they were removed from the ^{60}Co source. Although they were never above room temperature (which is no comparison to temperatures used in thermoluminescence), it may have been just enough to cause the defects to disappear. Finally, all irradiation experiments mentioned in Section 9.1 were performed using X-rays as the radiating element. In this experiment, γ rays were used. Perhaps γ rays induce defects that are not as stable as those induced by X-rays, especially at temperatures above 77K. Any or none of these factors may account for the fact that the radiation induced defects were not revealed by dielectric relaxation measurements.

9.5 Conclusion: As is apparent in Section 9.1, color mechanisms of calcite are not completely understood. This experiment showed that color changes can be induced in Swakopmund and Gallatin calcite by radiation. Whether or not these defects may be seen through relaxation measurements cannot be answered from this data. These defects did not appear in the dielectric signatures of the two calcites. However, poor experimental technique as well as natural mechanisms may be held accountable for that observation.

10. VANADYL PHOSPHATES:

10.1 Introduction: Vanadyl phosphate ($VOPO_4$) is a layered compound capable of being intercalated by a number of materials. Layered compounds have attracted considerable attention recently because of their potential applications as solid ionic conductors (or electrolytes), cathode materials, anisotropic electronic conductors, and catalysts.[43] One

of the most important heterogeneously catalyzed industrial reactions where the study of vanadyl phosphates has direct applications involves the process of allylic ammoxidation of propylene to acrylonitrile on various mixed metal oxides.[44] Water molecules ($VOPO_4 \cdot 2H_2O$) have a very pronounced effect on the physical and chemical properties of this compound. Additionally, proton donation within the layers of the compound has been speculated. Dielectric relaxation spectroscopy provides an ideal means for investigating the processes of such dynamic ions. Measurements of the complex impedance will yield the DC conductivity, hinting at clues that will lead to the understanding of systems with moveable ions.

10.2 Structure: Vanadyl phosphate has a lamellar structure composed of polymeric $(VOPO_4)_n$ layers. Those layers provide the host structure for the intercalation of various guest molecules, such as amines or alcohols. Additionally water can be reversibly intercalated leading to the formation of $VOPO_4 \cdot H_2O$ and $VOPO_4 \cdot 2H_2O$. Although several crystallographic structures exist for $VOPO_4 \cdot nH_2O$, work was only done with the $\alpha VOPO_4 \cdot 2H_2O$. It has a space group of P4/mmm corresponding to a tetragonal structure. Layers of $VOPO_4$ are comprised of chains which are linked together by the phosphate tetrahedron. It is between these layers that the water molecules are intercalated. The *c* parameter ranges from 4.11 Å to 6.30 Å to 7.41 Å for $VOPO_4 \cdot nH_2O$ where n=0,1,and 2, respectively.[45]

10.3 Experiment: The $VOPO_4 \cdot H_2O$ and $VOPO_4$ used for impedance measurements were prepared by heating $VOPO_4 \cdot 2H_2O$ for eight hours under flowing nitrogen at temperatures of 323K and 473K, respectively. Deuterated samples were prepared with 99% deuterated water and 85% D-3 phosphoric acid in a deuterated water solution. Sodium exchange

occurred in an aqueous solution of NaCl by stirring the solid $VOPO_4 \cdot 2H_2O$. Both the compound that underwent sodium exchange as well as its parent were characterized by 2% V(IV) reduction. measured by potentiometric titration. The redox value was in good agreement with other published values.[46]

To prepare the vanadyl phosphate for dielectric relaxation spectroscopy, the samples were ground and pressed into pellets. Both "two terminal" gold electrodes and "three terminal" aluminum electrodes were sputtered and vacuum evaporated onto the samples, respectively.[24] Measurements were made at 17 frequencies ranging from 10-10^5 Hz over a temperature range of 5.5-380K. The experimental setup was the same as described in Section 8.4. In the case of vanadyl phosphate, the real part of the dielectric constant was assumed to be on the order of 7 ± 2. At no time during data analysis were corrections made for the powdered instead of crystalline nature of the sample. This will result in somewhat large uncertainties.

10.4 Results: Two low temperature relaxations were seen in $VOPO_4 \cdot 2H_2O$ at 45K and 16K. In $VOPO_4 \cdot H_2O$, only the 16K relaxation is apparent. No relaxations are seen in $VOPO_4$. Plots of the imaginary part of the dielectric constant versus frequency are shown for all three types of compounds in Figure 10.1. The relaxation strength of the 16K peak increases with frequency while still retaining the same low temperature leading edge as seen in (a) and (b). Behavior such as this is usually characteristic of an unequivalent ion potential well system. In the deuterated forms of vanadyl phosphate, the position of the 16K relaxation peak is shifted to a higher temperature.

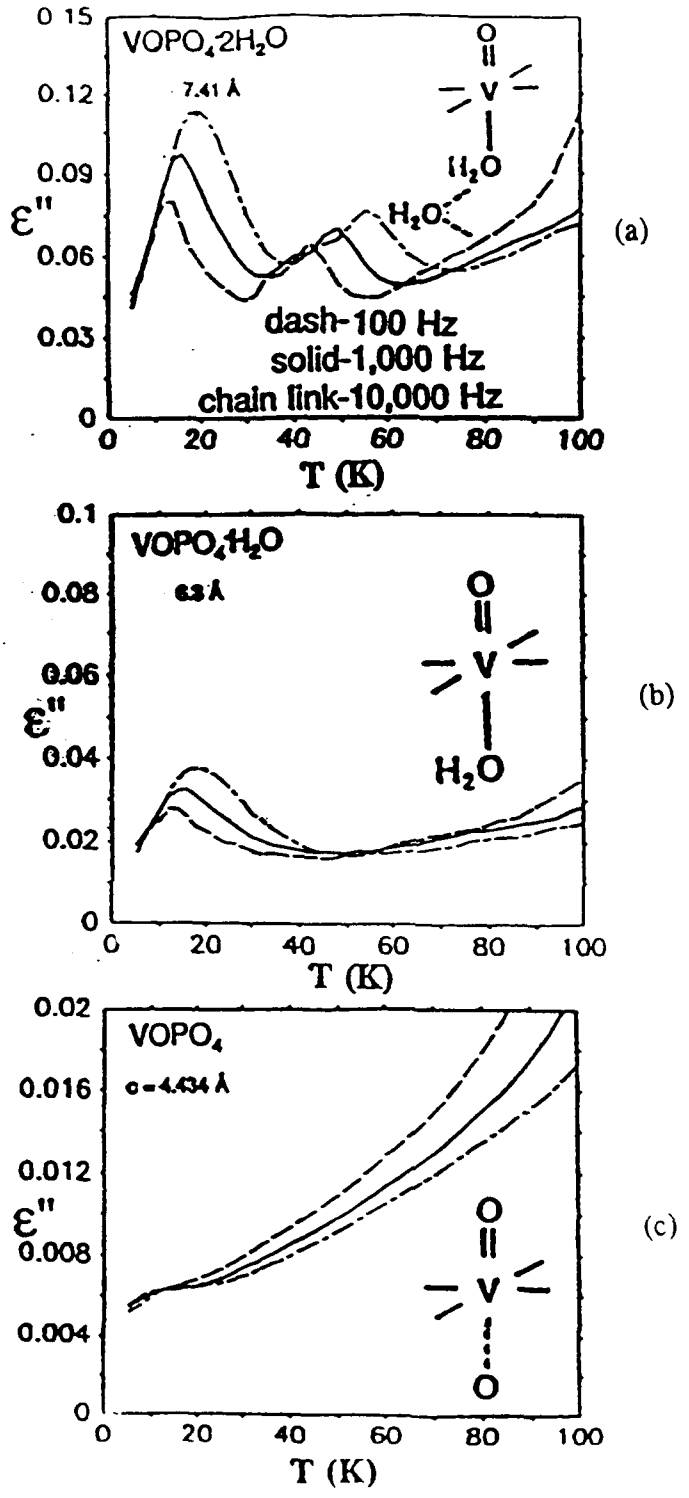

Figure 10.1 The imaginary part of the dielectric constant versus temperature for $VOPO_4 \cdot nH_2O$ where n = (2, 1, 0) as seen in (a), (b), and (c) respectively. Straight lines connect the data points. The c spacing (in Å) is listed in the upper left hand corner under the chemical formula

Unlike the 16K peak, the 45K peak exhibits Arrhenius behavior as previously described in Section 9. The least squares best fit values of energy and the $\log_{10}(\tau_o)$ were 0.080 eV and -12.0, respectively. This data is typical of standard dipolar reorientation phenomena. This relaxation is associated with the presence of the second hydrated water molecule that is usually found in the vicinity of the phosphate ion. When the water molecule is "boiled off," the 45 K relaxation is no longer seen. When the remaining coordinated water molecule is additionally "boiled off," the 16K relaxation disappears.

Finally, the electric conductivity of the compounds decreases as consecutive waters are lost from the layers. Deuterated conductivity values are less than the protonated values. Sodium ion exchange will cause the supernatant to become highly acidic. Conductivity will increase by a factor of 3 with the addition of just 2 mole % sodium. The results of electrical conductivity measurements are listed in Table 10.1. Note that the zero frequency value for the electrical conductivity was extrapolated at 294K (room temperature).

Table 10.1. Conductivity measurements of assorted vanadyl phosphate samples.

Sample Type	Conductivity (S/cm)
$VOPO_4 \cdot 2H_2O$	1.1×10^{-6}
$VOPO_4 \cdot H_2O$	3.0×10^{-7}
$VOPO_4$	1.0×10^{-8}
$VOPO_4 \cdot 2^2H_2O$	6.6×10^{-7}
$Na_{0.02}VOPO_4 \cdot 2H_2O$	3.6×10^{-6}
$Na_{0.14}VOPO_4 \cdot 1.9H_2O$	1.5×10^{-5}

10.5 Discussion: Four possible mechanisms were previously proposed to account for dielectric loss in the vanadyl pnictates: 1) a proton moving between a a pnictate oxygen and water located between the layers; 2) a proton being exchanged between the water coordinated to a vanadium and the water located between layers; 3) the reorientation of water dipoles; or 4) an electron moving between V(IV) and V(V) sites.

The last two possibilities can be eliminated immediately. The moving electron model must be ruled out because no change in the oxidation state of vanadium is observed with the loss of water. Water dipolar reorientation seems equally unlikely. Such reorientation would only be slightly diminished by sodium ion exchange. Only about 1% of the water would be displaced, but an 8-fold decrease is observed.

Some proton exchange between intralayer waters and proton sites is consistent with the data acquired. The deuterated samples do exhibit a pronounced isotope effect on the peak position of the imaginary part of the dielectric constant. This is an indication of hydrogen ion movement. Additionally, the ability of $VO(HPO_4)\cdot{}^1/_2H_2O$ to form a V(IV) - HPO_4 pair is evidence of proton exchange between the pnictate oxygen and the intralayer water. This is not the same as proton exchange between water coordinated to a vanadium and an intralayer water.

10.6 Conclusion: The only structural differences between the monohydrate and dihydrate vanadyl phosphates is the lack of the water molecule in the vicinity of the phosphate. This results in a reduction of the *c* spacing for the monohydrates. The disappearance of the 45K relaxation in the monohydrate is correlated to the loss of this water molecule. The 16K relaxation is correlated to the remaining water that is coordinated with a vanadium ion. Neither relaxations are found in $VOPO_4$. Dielectric loss

is associated with the mechanism of proton exchange between the pnictate oxygen and the intralayer water.

11. FUTURE APPLICATIONS:

11.1 Dielectric Characterization of Minerals: As clearly demonstrated by the results of this project, each type of calcite has its very own unique, characteristic dielectric signature or "fingerprint." This fingerprint may be a function of the geographical area in which the samples formed. For example, the dielectric signature of Swakopmund calcite from Africa is very different from the dielectric signature of Iceland Spar calcite from Mexico. These differences may be seen in Figures 8.3 and 8.2, respectively. By assembling a catalog of the different spectra, one will be able to determine in which geographic area an unknown calcite sample may have formed. Along similar lines, spectrum catalogs for different minerals may be used to determine the species membership of an unknown sample. Dielectric spectroscopy is not necessarily a destructive method of analysis. Spectrometers may be constructed to examine specimens of any shape.

11.2 Dielectric Dating: If correlations exist between radiation induced defects and the strength of various relaxations, then dielectric spectroscopy can be used to date inorganic specimens. The same radiation defect correlations are the present basis for dating by electron spin resonance[47] and by thermoluminescence. Assuming such correlations do exist, the height of the peaks which appear in plots of the imaginary part of the dielectric constant versus frequency will be directly proportional to the length of time that sample has been in existence providing the defects were

induced by cosmic radiation. Additional information involving the conditions under which the specimen was formed may result if the cause of the defect is known. For example, imagine that a type of defect can be induced in calcite by irradiation only under rather cold temperatures. The presence of that defect leads to the question of how the calcite became cold enough for it to be induced by cosmic radiation. One possible theory is that the defect may have been induced by incident cosmic radiation during the Ice Age.

12. SUMMARY:

The objective of this research was to examine and study the nature and configuration of some of the more prevalent defect complexes in a variety of calcite samples. Seven low temperature defect complexes in calcite have been observed and investigated using a variety of determinative techniques in conjunction with dielectric relaxation spectroscopy. The low temperature dielectric data obtained during this work has never before been seen in calcite. Defect complexes for three of those relaxations have been postulated. Additionally, the effects of hydrated water molecules on the dielectric properties of vanadyl phosphates have been studied. Two papers have been submitted for publication in conjunction with this project and other ongoing research at USNA. They are included in this report as Appendices I and II. The paper titled "Dielectric Loss in Vanadyl Pnictates" was published in the *Mat. Res. Soc. Symp. Proc.* (1991) 210 681-688 edited by G.A. Nazri, D.F. Shriver, R.A. Huggins, and A Balkanski. The paper titled "Dielectric Relaxation Spectroscopy in Calcite" has been submitted to the journal *Physics and Chemistry of Minerals.*

13. ACKNOWLEDGEMENTS:

The author would like to express his gratitude to the Scientific Research Department of the National Gallery of Art. In particular, he would especially like to thank Suzanne Lomax, Organic Chemist, and Deborah Rendahl, Conservation Scientist to the Systematic Catalog, for permitting him to take X-ray fluorescence measurements and perform the corresponding data analysis on their equipment.

The author also extends his heartfelt appreciation to Martin Nelson of the United States Naval Academy for carrying out the neutron activation analysis. His insights and contributions were too numerous to mention.

Most significant of all, the author thanks Mary Wintersgill, John Fontanella, Joseph Lomax, and Chris Coughlin for the countless hours each has devoted to this project. Without their devotion, patience, and dedication, none of this research would have been possible. A finite value cannot be placed on their contributions. Not only did they further the author's knowledge about the material contained herein, but they made the learning fun and enjoyable. Only very special people are capable of such an accomplishment.

---

[1]E.S. Dana. *Textbook of Mineralogy*. New York: John Wiley and Sons, Inc., 1932, p511-519.

[2]E.A. Wood. *Crystals and Light*. New York: Dover Publications, Inc., 1977, p69-71.

[3]S. Kondo, Y. Hiroshi, and K.Nakamura. "Optical Properties of Calcite in the Vacuum Ultraviolet." *J. Phys. Jap.* 34 (1973) 711.

[4]E.E. Whalstrom. *Optical Crystallography*. New York: John Wiley and Sons, 1979, p226-232.

[5]A.W. Nicol. *Physiochemical Methods of Mineral Analysis.* New York: Plenum Press, 1975, p87-107.

[6]J. Zussman. *Physical Methods in Determinative Mineralogy.* New York: Academic Press, 1967, p161-174, 475-487.

[7]S. A. Lomax, National Art Gallery Laboratory, Washington, D.C., private communication.

[8]M. Nakagawa, K. Fukunaga, M. Okada, and K. Atobe. "Lattice Defects in Thermoluminescent Calcite." *J. Lum.* 40-41 (1988) 345.

[9]D. Lapraz and P. Iacconi. "On Some Luminescent and Optical Properties of Synthetic Calcite Single Crystals." *Phy. Stat. Sol. A* 36 (1976) 603.

[10]J.S. Down, R. Flower, J.A. Strain, and P.D. Townsend. "Thermoluminescence Emission Spectra for Calcite and Iceland Spar." *Nucl. Tracks* 10 (1985) 581.

[11]R.L. Stux, and J.J. Sotera. *Atomic Absorption Methods Manual, Volume II, Methods Manual for Flameless Operation.* Wilmington, Massachusetts: Instrumentation Laboratory, Inc., 1975. p1-1 to 1-12.

[12]B.V. L'Vov. *Atomic Absorption Spectrochemical Analysis.* London: Adam Hilger Ltd., 1970, p118.

[13]J.W. Robinson. *Undergraduate Instrumental Analysis.* New York: Marcel Dekker, 1970, p183-184.

[14]N.H. Hartshorne and A. Stuart. *Practical Optical Crystallography.* London: Edward Arnold Ltd., 1969, p94-97.

[15]S.S. Nargolwalla and E.P. Przybylowicz. *Activation Analysis with Neutron Generators.* New York: John Wiley and Sons, 1973, p2-6.

[16]M.E. Nelson, United States Naval Academy, private communication.

[17]G. Erdtmann. *Neutron Activation Tables.* New York: Verlag Chemie, 1976, p19-131.

[18]ENGRWEPSDIVINST 11102.1F. 16 November, 1988.

[19]R.T. Conley. *Infrared Spectroscopy.* Boston: Allyn and Bacon, Inc. 1966, p6-7.

[20]Nicolet Analytical Instruments Technical Publication Department: P/N 269- 721903, 1986, p6-13.

[21]K. Nakamoto. *Infrared Spectra of Inorganic and Coordination Compounds.* New York: John Wiley and Sons, 1970, p170-178.

[22]Sadtler Research Laboratories. *Inorganics IR Grating Spectra.* Philadelphia, The Laboratories, 1965, p65.

[23]K.V. Rao and K. Suryanarayana Rao. "Dielectric Dispersion and its Temperature Variation in Calcite Single Crystals." *Z. Phys.* 216 (1968) 300.

[24]J. Toulouse, S. Ling, and A.S. Nowick. "Dielectric Relaxation of the Aluminum-hole Center in α-quartz: An Example of Phonon-assisted Tunneling." *Phys. Rev. B* 37 (1988) 7070.

[25]V.V. Daniel. *Dielectric Relaxation.* New York: Academic Press, 1967, p13-31.

[26]R. Shelby, J. Fontanella, and C. Andeen. "The Low Temperature Electrical Properties of Some Anisotropic Crystals." *J. Phys. Chem Solids* 41 (1980) 69.

[27]C. Andeen, D. Link and J. Fontanella, *Phys. Rev. B.* 16 (1977) 3762.

[28]J. Link, M.C. Wintersgill, J.J. Fontanella, V.E. Bean, and C.G. Andeen. "Pressure Variation of the Low-frequency Dielectric Constants of Some Anisotropic Crystals." *J. Appl. Phys.* 52 (1981) 936.

[29]C.P. Smith. *Dielectric Behavior and Structure.* New York: McGraw-Hill, 1955, p102.

[30]J.J. Fontanella, A.V. Chadwick, V. M. Carr, M.C. Wintersgill, and C.G.

Andeen. "Dielectric Relaxation Studies of Alkali-metal-doped Calcium Fluoride." *J. Phys. C: Solid St. Phys.* 13 (1980) 3457.

[31]J. Fontanella and C. Andeen. "The Dielectric Spectrum of Erbium Doped CaF_2." *J. Phys. C: Solid St. Phys.* 9 (1976) 1055.

[32]J.A. Saussmann. "Quantum Mechanical Theory of Barrier Crossings by Ions in Solids." *J. Phys. Chem. Solids.* 28 (1967) 1643.

[33]R. Pirc, B. Zeks, and P. Gosar. "Kinetics of the Alignment of $(O_2)^-$ Centers in Stressed Alkali Halide Crystals." *J. Phys. Chem. Solids.* 27 (1966) 1219.

[34]B.G. Dick and D. Strauch. "Theory of One- and Two-Phonon Reorientation Rates of Paraelectric Defects in Ionic Crystals." *Phys. Rev. B.* 2 (1970) 2200.

[35]H.B. Shore and L.M. Sander. "Calculation of Reorientation Rates of OH- in RbBr Using Accurate Phonon Spectra." *Phys. Rev. B.* 6 (1972) 1551.

[36]J. Cass, R.S. Kent, S.A. Marshall, and S.A. Zager. "Electron Spin Resonance Absorption Spectrum of $(HCO_3)^{-2}$ Molecule-Ions in Irradiated Single-Crystal Calcite." *J. Mag. Res.* 14 (1974) 170.

[37]R.D. Shannon. "Revised Effective Ionic Radii and Systematic Studies of Interatomic Distances in Halides and Chalcogenides" *Acta. Cryst.* 32 (1976) 751.

[38]S.A. Marshall, J.A. McMillan, and R.A. Serway. "Electron Spin Resonance Absorption Spectrum of Y^{+3} - Stabilized $(CO_3)^{-3}$Molecular-Ion in Single-Crystal Calcite." *J. Chem. Phys.* 48 (1967) 5131.

[39]T. Calderon, M Aguilar, R. Coy-yll. "Relationship Between Blue Color Damage in Calcite." *Rad. Eff. Lett.* 76 (1983) 187.

[40]M.C. Wintersgill. *Luminescence in LiF: Mg: Ti.* Doctor of Philosophy Thesis: University of Sussex: 1977, p9.

[41]V.M. Sergeev, N.F. Shunkin, and G.P. Barsanov. *Com. AKAD. USSR.*

231 (1976) 1222.

[42]K.V. Rao and S. Roy. "Thermoluminescence and Dielectric Loss in Calcite Single Crystals Irradiated by X-rays." *S. S. Comm.* 20 (1976) 941.

[43]M.R. Antionio, R.L. Barbour, and P.R. Blum. "Intralayer Coordination Environments of Iron, Cobalt, and Nickel in Vanadyl Phosphate Dihydrate, $VOPO_4 \cdot 2H_2O$, Intercalation Compounds." *Inorg. Chem.* 26 (1987) 1235.

[44]B. Schiøtt, K.A. Jørgensen, and R. Hoffmann. "On the Formation of Maleic Anhydride on a Vanadyl Pyrophosphate Surface: A Theoretical Study of the Mechanism." Office of Naval Research: Contract N00014-89-J-1052 (1990) Report No. 49.

[45]C. R'Kha, M.T. Vandenborre, and J. Livage. "Spectroscopic Study of Colloidal $VOPO_4 \cdot 2H_2O$." *J. Sol. St. Chem.* 63 (1986) 202.

[46]D. Ballutaud, E. Bordes, and P. Courtine. *Mat. Res. Bull.* 17 (1982) 519.

[47]A.M. Rossi and G. Poupeau. "Radiation-Induced Paramagnetic Species in Natural Calcite Speleothems." Centro Brasileiro de Pesquisas Fisicas, Rio de Janeiro (CBPF), RJ (Brazil). 1989.

APPENDIX I

"Dielectric Loss in Vanadyl Pnictates"

by

Joseph F. Lomax
Chemistry Department
U.S. Naval Academy
Annapolis, MD 21402

and

John J. Fontanella, Mary C. Wintersgill, and Anthony J. Kotarski
Physics Department
U.S. Naval Academy
Annapolis, MD 21402

Joseph F. Lomax*, John J. Fontanella**, Mary C. Wintersgill** and Anthony Kotarski**
* Chemistry Department, United States Naval Academy, Annapolis, MD 21402
** Physics Department, United States Naval Academy, Annapolis, MD 21402

ABSTRACT

The results of audio frequency complex impedance studies for vanadyl phosphate and its hydrates ($VOPO_4 \cdot nH_2O$; n=0,1,2) are reported. Measurements were made at seventeen frequencies between 10 and 10^5 Hz over the temperature range 5.5-380K. Two low-temperature features were observed and are correlated with particular water species between the $VOPO_4$ layers. In light of chemical evidence and complex impedance measurements on related compounds, it is speculated that $VOPcO_4 \cdot nH_2O$ (Pc = P, As) can be thought of as a mixed nonstoichiometric compound $[VO(HPcO4)]_x[VOPcO_4]_{1-x} \cdot nH_2O$ and the solid Brønsted acid nature of the compound is related to proton movement between layer pnictates and intralayer waters.

INTRODUCTION

Vanadium phosphorous oxides are used as selective, mild oxidation catalysts (e.g. conversion of butane to maleic anhydride)[1]. Vanadyl phosphate ($VOPO_4$) is a layered compound that can be intercalated by a host of materials[2,3,4]. The wide variety of reaction that vandyl phosphate can accomplish is made possible by virtue of its available coordination site (for Lewis acid/base reactions), and its reversible V^{4+}/V^{5+} redox couple. The vanadium is seated in a distorted octahedron of oxygens where each of the equatorial oxygens is from a corner-shared phosphate. The double bonded axial oxygen fills the final coordination spot in the adjacent layer in the dehydrated form (interlayer spacing = 4.434 Å). In the hydrated forms the final coordination spot is filled by a water. The second water in the $VOPO_4 \cdot 2H_2O$ [5,6] is found in the vicinity of the phosphate, as seen in Figure 1 (interlayer spacing = 7.41 Å).

Clearly water has a profound effect on the $VOPO_4 \cdot 2H_2O$ structure, and, one would expect, the chemical and physical properties of not only the this compound. but its

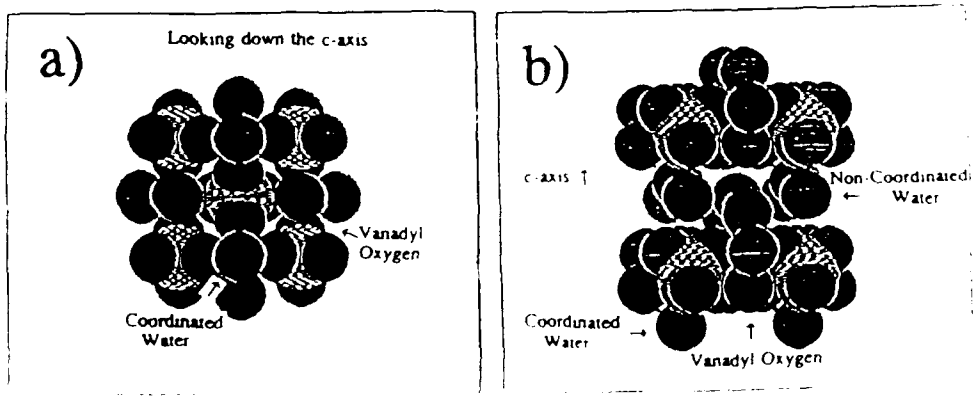

Figure 1. View of part of a Vandyl Phosphate layer a) down the c-axis and b) with a view of the intralayer waters.

intercalation compounds. The nature of the water between the layers has been a point of discussion in the literature[7,8]. It has been speculated that the acidic nature of $VOPO_4 \cdot 2H_2O$ extends past the Lewis acidity of the vanadium to proton donation. The spectroscopy hints of protons associated with one or more of waters (to form a hydronium ion), vanadyl oxygens or phosphate oxygens. Within and between the layers, any proton movement must be a dynamic process of protons being donated and accepted. AC impedance measurements are ideally suited for investigating such dynamic ion processes. It has a wide dynamic range, it can provide information the nature and energetics of ion movement processes, and can yield the dc conductivity.

In addition to its varied reactivity and numerous compounds that it forms, vanadyl phosphate has many of the characteristic of a good model compound, particularly in layered oxides structure where ion movement is restricted to one or two dimensions. It has a well characterized structure, and it can be identified by a variety of physical methods, such as ir, x-ray powder diffraction, thermal gravimetric analysis (TGA), potentiometric titrations, and elemental analysis. With ac impedance measurements, structural and chemical knowledge one can develop an understanding of systems with moveable ions.

EXPERIMENTAL

$VOPO_4 \cdot 2H_2O$, products of its redox intercalation and $VO(HPO_4) \cdot \frac{1}{2}H_2O$ were prepared by published procedures[1-3,9]. The batch of $VOPO_4 \cdot 2H_2O$ used to make samples for impedance measurements was treated to make the $VOPO_4 \cdot H_2O$ and $VOPO_4$ samples for analogous studies by heating the dihydrate for 8 h under flowing nitrogen at 50° C and 200° C, respectively. Compounds were characterized by TGA, potentiometric titrimetry and IR spectroscopy[10]. The deuterated sample was prepared with ^2H_2O (99% ^2H) and 85% D-3 phosphoric acid in ^2H_2O. Sodium exchange was accomplished by stirring the solid $VOPO_4 \cdot 2H_2O$ in aqueous NaCl. The sodium exchanged compound, as well as the parent $VOPO_4 \cdot 2H_2O$, have 2 % V(IV) as measured by potentiometric titrimetry in good agreement with published esr measurements[11]. $VOAsO_4 \cdot 2H_2O$ powder was made by a published procedure and the single crystals (as viewed by crossed-polarizing microscopy) formed by slow evaporation. Although water loss from $VOAsO_4 \cdot 2H_2O$ crystal surfaces has made X-ray crystallography difficult, ac impedance measurements still reflect the bulk characteristics of the material; this conclusion is supported by comparison of the crystal to the pressed powder sample.

Microcrystalline powders were ground and pressed into pellets. Usually, gold electrodes were sputtered onto samples in a two-terminal configuration. However, aluminum electrodes were vacuum deposited onto some samples to rule out electrode effects.

Previously published methods were used to make audio frequency complex impedance measurements and transform the results to the real and imaginary parts of the dielectric constant, ε' and ε'', respectively.[12] For the present materials, the dielectric constant at low temperatures is on the order of 7 ± 2. The large uncertainty arises from the fact that no attempt was made to correct for either the powder nature of the samples, or the two terminal nature of the measurements.

Two low temperature relaxations were found for the vanadyl phosphate hydrates. Each relaxation correlates with a particular species of water. Typical results are shown in Figure 2 which exhibits relaxations at 1000 Hz for the dihydrate at 16K (Type I) and 45K (Type II). Only Type I relaxation is observed in $VOPO_4 \cdot H_2O$ and $VOAsO_4 \cdot 2H_2O$. No features were observed in measurements of $VOPO_4$ or the related $VO(HPO_4) \cdot \frac{1}{2}H_2O$.

The Type II relaxation exhibits features typical of standard dipole reorientation. The relaxation time, τ, was calculated as the inverse of ω_{max}, the frequency of the maximum ε'' value. Reported relaxation times assume that $\omega_{max}\,\tau = 1$. The relaxation was found to exhibit Arrhenius behavior, and thus the expression:

$$\tau = \tau_0 e^{E/kT} \qquad (1)$$

was optimized to the data. The least-squares best fit parameters were found to be E = 0.080(2) eV and $\log_{10}\tau_0 = -12.0$.

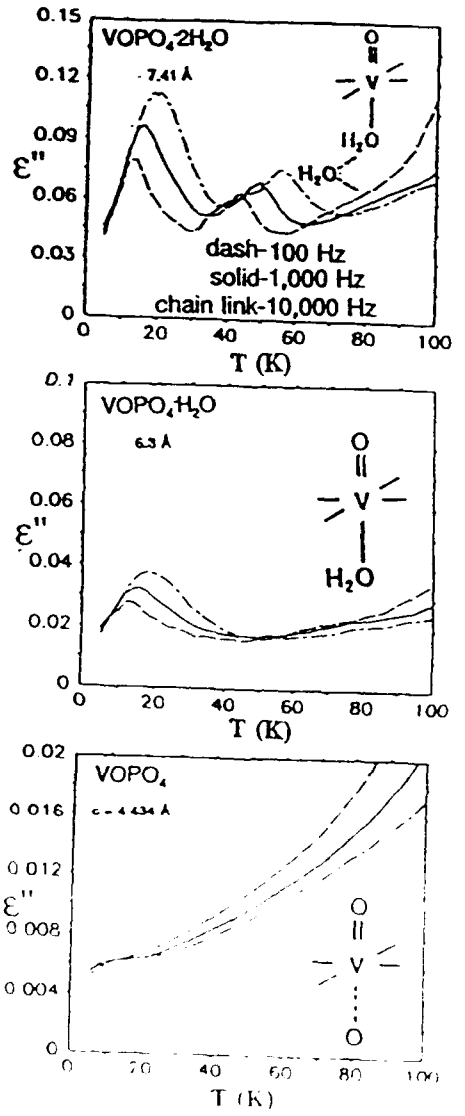

Figure 2 Low temperature dielectric loss for $VOPO_4 \cdot nH_2O$ (n = 2,1,0)

The Type I relaxation is more difficult to describe quantitatively. The relaxation strength increases with frequency, and the same low temperature leading edge is followed at every frequency. This is characteristic of an inequivalent-well system. In fact, the increase can be explained with a well inequivalency of 0.01 eV, and the 1000 Hz peak position is reproduced with an average barrier height of 0.02 eV, assuming a pre-exponential of 10^{12}s (as was obtained for the Type II relaxation). However, this model does not explain the width of the peaks. As a consequence, a model with a distribution of such wells will be needed for a proper treatment of the Type I relaxation.

As seen in Table I, the temperatures at which Type I peaks occur are the same for $VOPO_4 \cdot 2H_2O$ and $VOPO_4 \cdot H_2O$. However, the Type I is shifted to a higher temperature for the deuterated vanadyl phosphate compared to the protonated forms. This is evidence for proton motion as the effect of increasing mass (proton to deuteron) should be to increase the peak temperature (or equivalently, decrease the frequency at a given temperature). The isostructural $VOAsO_4 \cdot 2H_2O$ shows similar Type I peaks for both crystalline and polycrystalline pressed powder samples

However, these peaks are consistently at lower temperature than observed for $VOPO_4 \cdot 2H_2O$. In this case no Type II peaks are observed.

Table I shows that the extrapolated zero frequency electric conductivity of $VOPO_4 \cdot 2H_2O$ at 294K falls with consecutive water loss from between the layers. Thermal cycling of the sample demonstrates that the higher conductivity of the hydrates is associated with the water. Upon warming the sample of $VOPO_4 \cdot 2H_2O$ above the dehydration temperature, the conductivity smoothly drops to the lower value indicative of $VOPO_4$. The value for the deuterated form conveniently falls below that of the protonated form. Though an isotope effect is implied, batch to batch sample variation might also account for such an effect. In contrast to this intriguing behavior, the dielectric loss in the corresponding V(IV) compound, $VO(HPO_4) \cdot \frac{1}{2}H_2O$, is featureless. Also, its conductivity is a factor of 250 lower than that observed for even $VOPO_4$.

Stirring solid $VOPO_4 \cdot 2H_2O$ with aqueous NaCl, results in sodium ion exchange and the supernatant becomes highly acidic. While the peak positions in the Type I ε" are the same, their intensities are reduced to 1/8 of the original and the Type II peaks disappear altogether. However, the conductivity increases by a factor of 3 with an addition of only 2 mole % of sodium. This increase in conductivity is similar though proportionately smaller than that observed among sodium redox intercalated compounds. In these compounds, one of which is given in Table I, the Type I feature is extinguished.

Table I. Conductivity[†] and Dielectric Loss Behavior of Selected Samples.

	Conductivity ($S \cdot cm^{-1}$)	Temperature (K) of Type I peak ε" @ Hz: 10^2	10^3	10^4
$VOPO_4 \cdot 2H_2O$	1.1×10^{-6}	13	16	20
$VOPO_4 \cdot H_2O$	3.0×10^{-7}	13	16	20
$VOPO_4$	1.0×10^{-8}	no peaks		
$VOPO_4 \cdot 2^2H_2O$	6.6×10^{-7}	17	22	26
$VOAsO_4 \cdot 2H_2O$	3×10^{-9}	10.5	12	14
$Na_{0.02}VOPO_4 \cdot 2H_2O$	3.6×10^{-6}	13	16	20
$Na_{0.14}VOPO_4 \cdot 1.9H_2O$	1.5×10^{-5}	no peaks		
$VO(HPO_4) \cdot \frac{1}{2}H_2O$	4×10^{-11}	no peaks		

[†] Extrapolated zero frequency electrical conductivity at 294 K

DISCUSSION

The only structural difference between the monohydrate and the dihydrate are the lack of the water molecule in position B. This results in a reduction in the *c* spacing. The disappearance of the Type II relaxation in the monohydrate is correlated with the loss of this water. The Type I relaxation correlates with the remaining water in position A of both mono- and dihydrate, and is not found in $VOPO_4$.

Prior to this study, four mechanisms for dielectric loss in the native vanadyl pnictates could be proposed: 1) an electron could be moving between V(IV) site and V(V) sites, 2) a reorientation of the water dipoles may occur; 3) a proton could be exchanged between water coordinated to a vanadium and water between layers, or 4) a proton could move between a pnictate oxygen and water between the layers.

The first two are readily eliminated. No change in vanadium oxidation state is observed upon loss of water, even though Type I and II features are lost, thus ruling out

1). Water dipole reorientation would only be slightly diminished by sodium ion exchange since only about 1% of the water is displaced. However, an 8-fold decrease observed Water dipole reorientation will not account for this and seems highly unlikely.

Some proton exchange between a proton site and intralayer waters is consistent with the data. The fact that the deuterated samples exhibit a pronounced isotope effect on the peak position of ε" is consistent with hydrogen ion movement. A proton (or hydronium ion) associated with a water would more likely be a bound particle than a sodium ion, for which intercalation compounds show no bound-particle behavior. As the low temperature features are either extinguished or greatly diminished and the conductivity is increased upon addition of only 2 mole % of sodium (the same mole % as the V(IV)), these protons are correlated with V(IV) centers. One might the speculate that the proton movement may be associated with the acid nature of the V(IV). However, this is counterintuitive as one would expect that the more highly charged V(V) center would be more acidic than the V(IV). Also, it might be thought that the less basic arsenate would temper the acidity of the V(IV) less than the phosphate, and would induce a higher energy transition for proton exchange. However, as seen in Table I, the Type I loss for $VOAsO_4 \cdot 2H_2O$ is at lower temperature (and energy) than that for $VOPO_4 \cdot 2H_2O$.

A proton would be more tightly bound to a phosphate than to an arsenate following the trend in Type I dielectric loss. The less acidic V(IV) would diminish the proton-accepting ability of the phosphate less than V(V). This suggests that the proton exchange occurs between the pnictate oxygen and an intralayer water, not between water coordinated to a vanadium and intralayer water. This is supported by noting the ability to form a V(IV)-HPO_4 pair is seen in $VO(HPO_4) \cdot \frac{1}{2}H_2O$. The remaining difficulty is to explain why $VO(HPO_4) \cdot \frac{1}{2}H_2O$ has no low temperature dielectric features or conductivity.

The structure of $VOPO_4 \cdot 2H_2O$ has four corner sharing phosphate oxygens forming an equatorial vertices of psuedooctahedral vanadiums. However, the HPO_4 unit of $VO(HPO_4) \cdot \frac{1}{2}H_2O$ has only three corner sharing oxygens with the other oxygen bonding to the hydrogen. At a level of only 2 mole %, HPO_4 units may not even disrupt the fully corner sharing nature of the phosphate in $VOPO_4 \cdot 2H_2O$ and could be thought of as a charged defect in the solid. In $VO(HPO_4) \cdot \frac{1}{2}H_2O$, however, this unit is not a defect, but the phosphate bound protons are without a nearby equivalent site to move to or any clear path for conductivity. Thus it is expected that $VO(HPO_4) \cdot \frac{1}{2}H_2O$ would have no bound charge particle motion and would be an ionic insulator.

CONCLUSION

The hydrates of the vanadyl pnictates are characterized by a Brønsted acid character which manifests itself in dielectric loss features at low temperature and in chemical evidence. It is speculated that the acidity is a factor of hydrogenphosphate units associated with V(IV) centers. An alternate formulation of these compounds could therefore be $[VO(HPcO4)]x[VOPcO_4]_{1-x} \cdot nH_2O$

This study has found interesting low temperature features in the vanadyl pnictates, such as the unusual inequivalent well system. More importantly, it gives support to the utility of low temperature complex impedance measurements in the rationalization of chemical behavior, and determination of the environment and energetics of layered materials. Further investigation of other layered and intercalation systems is ongoing.

ACKNOWLEDGEMENTS

This work was supported in part by the Naval Academy Research Council and the National Science Foundation.

REFERENCES

1 G. Centi, F. Trifiro, J.R. Ebner, V.M. Franchetti, Chem. Rev. 88, 55 (1988) and references therein.
2 J.W. Johnson, A.J. Jacobson, J.F. Brody, S.M. Rich, Inorg. Chem. 21, 3820 (1982).
3 A.J. Jacobson, J.W. Johnson, J.F. Brody, J.C. Scanlon, J.T. Lewandowski, Inorg. Chem. 24, 1782 (1985).
4 J.W. Johnson, A.J. Jacobson, Angew. Chem., Int. Ed. Engl. 22, 412 (1983).
5 Crystal coordinates from H.R. Tietze Aust. J. Chem. 34, 2035 (1981).
6 M. Tachez, F. Tanobald, J. Bernard, A.W. Hewat, Rev. Chim. Miner., 19, 291 (1982).
7 C. R'Kha, M.T. Vandenborre, J. Livage, R. Prost, E. Huard, J. Solid State Chem. 63, 202 (1986).
8 N. Casañ, P. Amorós, R. Ibañez, E. Martínez-Tamayo, A. Beltrán-Porter, D. Beltrán-Porter, J. Inclusion Phenom. 6, 193 (1988).
9 J.W. Johnson, D.C. Johnston, A.J. Jacobson, J.F. Brody, J. Amer. Chem. Soc., 106, 8123 (1984).
10 M.R. Antonio, R.L. Barbour, P.R. Blum, Inorg. Chem. 26, 1235 (1987).
11 D. Ballutaud, E. Bordes, P. Courtine, Mater. Res. Bull., 17, 519 (1982).
12 J.J. Fontanella, M.C. Wintersgill, M.K. Smith, J. Semancik, C.G. Andeen, J. Appl. Phys. 60, 2665 (1986).

APPENDIX II

"Dielectric Relaxation Spectroscopy in Calcite"

by

A.J. Kotarski, M.C. Wintersgill
J.J. Fontanella, C.S. Coughlin
Physics Department
U.S. Naval Academy
Annapolis, MD 21402

and

Joseph F. Lomax
Chemistry Department
U.S. Naval Academy
Annapolis, MD 21402

DIELECTRIC RELAXATION SPECTROSCOPY IN CALCITE

A.J. Kotarski, M. C. Wintersgill
J. J. Fontanella, C. S. Coughlin
Physics Department
U. S. Naval Academy
Annapolis, MD 21402-5026

J. F. Lomax
Chemistry Department
U. S. Naval Academy
Annapolis, MD 21402-5026

ABSTRACT

Audio frequency complex impedance measurements have been carried out in vacuum over the temperature range 5.5 - 300 K on three types of naturally occurring calcite. The measurements were made with the electric field perpendicular to the cleavage planes and both parallel and perpendicular to the c-axis. All materials exhibit a 1000 Hz relaxation peak parallel to the optic axis with a peak position of about 38K. This relaxation is strongest in the Swakopmund (blue) calcite and appears to be associated with a yttrium - $(CO_3)^{-3}$ ion pair. The Gallatin Mt. and the Mexican samples show a relaxation at very low temperatures perpendicular to the c-axis (1000 Hz peak at about 7K) which exhibits characteristics of a tunnelling phenomenon and which is attributed to proton motion. Five other relaxations are observed and their possible origins are discussed. Finally, a quantitative description of most of the relaxations is given.

INTRODUCTION

In spite of the technological importance of calcite, there appear to have been relatively few reports of the imaginary part of the dielectric constant (dielectric loss), ε''. In the one paper which has been published (Rao and Rao 1968) the work only extends from 80K upward and, no relaxation peaks were reported. However, a preliminary report of ITC (ionic thermocurrent) studies in calcite has been given (de Lima et al. 1988). In addition, in a paper by one of the authors (Shelby et al., 1980) several relaxation peaks in calcite were mentioned but were not described in detail as the purpose of that paper was to establish values for the real part of the dielectric constant, ε'. In another paper (Link et al. 1981), one of the authors has reported the effect of high pressure on the dielectric constant, but again, dielectric loss was not reported.

In fact, dielectric loss is a powerful technique for detecting and characterizing dipolar defects in materials. For example, the authors have carried out extensive dielectric spectroscopy in fluorite and isomorphic materials (Andeen et al. 1977, 1981; Figueroa et al. 1984a,b, 1987; Fontanella and Andeen 1976; Fontanella et al, 1981, 1983; Kimble et al. 1982; and references therein) containing aliovalent dopant ions. A large number of relaxations were catalogued and used to identify and characterize various defects in those materials. In an attempt to obtain information concerning defects in calcite, dielectric relaxation studies have been carried out.

EXPERIMENT

Naturally occurring calcite from Montana (Gallatin Mountain), Southwest Africa (Swakopmund), and Mexico (Creel, Chihuahua) were obtained from Ward's Natural Science Establishment, Inc. of Rochester, New York. The Swakopmund samples were of a bluish-white marble color with an opaque nature; the Mexican samples were of the clear Iceland Spar variety; and the Gallatin samples were of a faint yellow color with only a slightly opaque nature. Platelet-shaped samples were either cleaved or were cut with the c-axis (optic-axis) parallel or perpendicular to the large face. The samples were all less than 1.5 mm thick and of various shapes.

Aluminum electrodes were vacuum evaporated onto the surfaces in either two-terminal or three-terminal configuration (with a 9mm central guarded region in the core of the three terminal configuration). In most cases the samples were finished using a 4/0 grit Carborundun polishing paper. Complex impedance measurements were then carried out using a CGA-82 microprocessor controlled bridge which operates at seventeen frequencies between 10 and 10^5 Hz. Temperatures over the range 4.5-380K were carried out in a precision Cryogenics CT-14 dewar controlled by a Lake Shore Cryotronics DRC-82 temperature controller using a silicon diode. Further experimental details are given elsewhere (Andeen et al. 1977).

The resultant values of the capacitance, C, and the conductance divided by the angular frequency, G/ω, were then transformed to the imaginary part of the dielectric constant (dielectric loss) parallel to the c-axis, ε''_{33}, and perpendicular to the c-axis, ε''_{11} as follows. The values of the

real part of the dielectric constant, ε_i', at about 5.5K were set equal to 8.219 and 7.633 perpendicular and parallel to the optic axis respectively (Shelby et al 1980). The value for the cleaved samples was taken to be 7.926. As corrections for thermal expansion make a small contribution to dielectric loss, it was assumed that the relative change in the dielectric constant is equal to the relative change in capacitance. Finally, the imaginary part of the dielectric constant was calculated using the definition:

$$\varepsilon_{ii}'' = \frac{G\varepsilon_{ii}'}{\omega C} \qquad (1)$$

Further details of experimental techniques used to determine values for the complex dielectric constant may be found elsewhere (Andeen et al.,1977).

In order to gain some information concerning the impurity content of the samples, Fourier transform infrared (FTIR), x-ray fluorescence (XRF) and 14.5 MeV neutron activation analyses (NAA) of the samples were carried out.

RESULTS

The results for the imaginary part of the dielectric constant for cleaved samples of each type of calcite at a frequency of 10^3 Hz and over a temperature range of 4.8-230K are shown in Figure 1. The principal relaxations for each material are apparent and their peak heights are given in Table 1. Six relaxations were observed for the Mexican material (dashed line) at temperatures of 7K, 13K, 38K, 121K, 168K and 220K and the Gallatin sample exibited six relaxations at temperatures of 7K, 13K, 21K,

38K, 168K and 220K. The Swakopmund sample (solid line) exhibited three principal relaxations occurring at temperatures of 13K, 21K, and 38K respectively. Interestingly, the least complicated spectrum is exhibited by the Swakopmund material which, on the basis of the NAA studies, contains the largest variety of impurities. This implies that many of the impurities in the Swakopmund material do not give rise to a dipolar complex. The reason for this behavior will be discussed later.

In order to obtain information concerning the symmetry of the defect sites, measurements were carried out both parallel and perpendicular to the optic axis on some of the materials. Typical results for the 1000 Hz loss parallel and perpendicular to the optic axis are shown in Figure 2. It is clear that the 13K relaxation is only seen when the optic axis was oriented perpendicular to the electric field while the 38K peak appears parallel to the optic axis. (Traces of the 38K peak are also observed perpendicular to the c-axis but as the strength was at least 50 times weaker than parallel to the c-axis this is attributed to uncertainty in the actual orientation.) Next, it is clear from Figure 2 that the 121K peak is only observable parallel to the optic axis. The 168K relaxation, on the other hand, is observable both parallel and perpendicular to the optic axis, being about a factor of 3 stronger along the axis. Further, as is apparent from Figure 2, the relaxation perpendicular to the optic axis is complex appearing to be composed of at least two closely-spaced relaxations. Finally, when the electric field is perpendicular to the c-axis, a very low temperature relaxation, 7K, is observed.

In order to evaluate each of the relaxations quantitatively, a characteristic relaxation time, τ, was determined for each relaxation

observed. The procedure was to construct plots of ε" vs applied frequency as shown for a typical data set in Figure 4. The relaxation time was taken to be the reciprocal of the peak position i.e. $\omega_{max}\tau=1$. Best values of ω_{max} were obtained by best-fitting the empirical Cole-Cole expression (Smythe 1955):

$$\varepsilon'' = \frac{(\varepsilon_L' - \varepsilon_H')\cos(\alpha\pi/2)}{2\{\cosh[(1-\alpha)x] + \sin(\alpha\pi/2)\}} \qquad (2)$$

to the data. α is the constant Cole-Cole parameter, ε''_L and ε''_H are the 'low' and 'high' frequency limits of the dielectric constant where 'low' and 'high' mean relative to the effects of the relaxation only and $x = \ln(\omega\tau)$. The best-fit results showed that:

$$\varepsilon_L' - \varepsilon_H' = \frac{A}{T} \qquad (3)$$

where A is a constant known as the dipole strength. The value of A is given by:

$$A=Np^2/3\varepsilon_o k_b \qquad (4)$$

N is the concentration of the dipoles, p is the dipole moment and ε_o is the permittivity of free space.

In order to emphasize the sensitivity of the dielectric relaxation technique, it is of interest to calculate typical concentrations for the defects reported in the present work. For example, by comparison with data for erbium in fluorite (Fontanella and Andeen 1976), for A=0.005 which is typical for a weak peak, the concentration of dipoles would be on the order of 5×10^{-6} % or 50 ppb. This is on the order of the peak height so that the

sensitivity is at the ppb level.

Finally, Arrhenius plots were made for each relaxation. Figure 5 shows results from the 38K relaxation which are typical for all but the 7K relaxation. It is clear that Arrhenius behavior is observed and thus the equation:

$$\ln(\tau) = E / k_b T + \ln(\tau_o) \qquad (5)$$

was best-fit to the data where appropriate. E and τ_o are constants known as the activation enthalpy and the reciprocal frequency factor, respectively, and k_b is Boltzmann's constant. The best-fit parameters from both equations (2) and (5) are listed in Table 2. For the samples which exhibit Arrhenius behavior, all of the values for $\log_{10}(\tau_o)$ are on the order of -12. This is reasonable as it is typical of the reciprocal of a lattice vibrational frequency.

However, deviation from Arrhenius behavior was observed for two relaxations. As shown in Figure 6, the Arrhenius plot for the 7K relaxation in both the Mexican (Iceland Spar) and Gallatin calcites is non-linear. The shape of the curves is characteristic of quantum mechanical tunnelling and such phenomena are usually treated by the addition of a term linear in the temperature (Toulouse and Nowick, 1988):

$$1/\tau = BT + (1/\tau_o)\exp(-E/k_b T) \qquad (6)$$

The results of the best-fit parameters are listed in Table 2. The values of $\log_{10}(\tau_o)$ for the 7K relaxation in the Mexican (Iceland Spar) and Gallatin calcites, -9.2 and -8, are somewhat less negative than for the other

relaxations all of which are on the order of -12. Those values are probably an artifact of the fitting procedure and the extent of the data since, as can be seen in Figure 6, the data dominated by the Arrhenius portion of the curve were obtained over a limited range of temperatures.

DISCUSSION

General Observations

The results in Table 1 show that the spectra for samples from a particular origin are quite similar, the existence of particular sequence of peaks being characteristic of the origin of the samples. The data in Figure 5, where an Arrhenius plot of the relaxation times (peak positions) for various samples is shown, emphasize how well-defined the relaxations are. It is clear that data for a particular peak in different materials are virtually indistinguishable and thus the activation enthalpy and reciprocal frequency factor are unique for a given process. However, as might be expected, the peak heights vary greatly from sample to sample. That implies that the concentration of defects varies greatly from sample to sample, as is expected for naturally occuring materials.

38K Relaxation

The 38K relaxation, which is observed parallel and not perpendicular to the c-axis, is the only relaxation common to all three materials for the temperature range covered by the present experiment. Consequently, the impurity responsible for this relaxation should be observed in all three materials. The NAA and XRF studies indicated that there are several impurities which are found in all three materials. However, many of the impurities are unlikely to give rise to a dipolar defect. For example, strontium is found in all materials. It is not likely to give rise to a relaxation peak as it is substitutional for calcium and from size considerations is not likely to sit "off-center." In fact, only very small

isovalent impurities are likely to give rise to dielectric relaxation as they may sit in "off-center" sites and thus may move between equivalent "off-center" sites with the application of an electric field. This will be considered later.

In fact, the strongest evidence is that the 38K relaxation is associated with a defect site containing yttrium, which is an aliovalent cation. The reason that such defects give rise to electrical relaxation is that when yttrium is present either substitutionally (for calcium) or interstitially, charge compensation is necessary and usually takes place via the addition of oppositely charged entities to the lattice. When the charge compensators are located near the yttrium a dipole results which can usually reorient with the application of an electric field, hence the origin of a relaxation peak.

The NAA studies showed that yttrium is found in all materials and has the lowest concentration in the Mexican material. This correlates with the strength of the 38K relaxation which is weakest in the Mexican material. In fact, a specific defect center containing yttrium has been proposed on the basis of various electron spin resonance studies (Marshall et al. 1967). It has been concluded that a $(CO_3)^{-3}$ forms in the vicinity of the Y^{3+} and that this defect is stable up to at least 500K. Further, Calderon et al. (1983) have shown that unirradiated blue (similar to Swakopmund material) samples exhibit a 500K thermoluminescence (TL) peak. Both they and Lapraz and Iaconi (1976) associate that peak with defect (such as Y^{3+}) stabilized $(CO_3)^{-3}$ ions so that large numbers of such sites can exist in unirradiated, natural calcite. The problem which remains is to determine whether such a site can reorient under the application of an electric field and, more specifically, if

the reorientation will take place along the c-axis. Marshall et al. (1967) describe the yttrium ion as "an interstitial with equal probablility of being slightly displaced above or below the plane of the normal divalent carbonate ions." Consequently, the equivalent positions for the yttrium ion are those which are required for the 38K relaxation as they are located along the c-axis. It will be of interest to determine whether the energy barrier for the motion of yttrium ions between equivalent sites can account for the activation enthalpy of 0.063 eV which is observed for the 38K relaxation.

The possible correlation between the 500K TL peak and the 38K relaxation suggests several experiments. For example, it would be of interest to heat the samples above 500K to look for any effect on the 38K relaxation. The reason, of course, is that once a thermoluminescence peak is observed, that defect center is destroyed and thus the 38K relaxation should disappear if it is correlated with the 500K TL peak. Such experiments are underway. In the event that the correlation is verified, one consequence is of particular interest. Specifically, dielectric relaxation would then provide a non-destructive (either to the radiation effects or the physical properties) method for evaluating radiation effects in calcite and hence would be of interest in dating.

13K Relaxation

The 13K relaxation is observed in the same materials as the 38K relaxation, though it is barely detectable in the cleaved Mexican samples. However, the symmetry is opposite that of the 38K relaxation in that the 13K relaxation is only observed perpendicular and not parallel to the c-axis.

Consequently, it is of interest to speculate that this relaxation is associated with a different yttrium - $(CO_3)^{-3}$ ion pair. In fact, Marshall et al. (1967) mention 24 centers about an order of magnitude lower in concentration that the yttrium - $(CO_3)^{-3}$ ion pair discussed in relation to the 38K relaxation. The type of center which might account for the 13K relaxation is a center based on a substitutional yttrium rather than an interstitial. The motion responsible for the 13K relaxation is proposed to be jumps of the $(CO_3)^{-3}$ ion in the planes of $(CO_3)^{-2}$ ions perpendicular to the c-axis. The reason that this model is interesting is that it would be expected that the energy barrier to motion in the plane of the $(CO_3)^{-2}$ ions would be quite small thus explaining the very low (0.024 eV) activation enthalpy of the 13K relaxation. In fact, at the lowest temperatures, the 13K relaxation shows indications of the onset of tunnelling which would be consistent with electron motion at low temperatures.

7K Relaxation

As has been discussed previously, the 7K relaxation exhibits interesting non-Arrhenius behavior characteristic of tunnelling. This suggests that the dipole reorientation may be due to the motion of electrons or of a small ion such as a proton. The FTIR studies revealed two possible origins for the 7K relaxation. First, via the absorption at 3550 cm^{-1} (2.8μm), it was found that the Mexican and Gallatin Mt. materials contain about the same amount of hydroxyl ions and that the Swakopmund sample contains significantly less. Second, the FTIR studies in the vicinity of 2600 cm^{-1} showed similar concentrations for the bicarbonate ion though the

interpretation of the data is not as clear as that for the hydroxyl ions. However, Cass et al. (1974) have obtained evidence for and justified the existence of bicarbonate ions in naturally occurring calcite. It is proposed that the bicarbonate ion would enter the lattice in conjuction with a monovalent substitutional such as an alkali metal ion.

Since the 7K relaxation is not observed in the Swakopmund sample, the FTIR studies suggest that either hydroxyl or bicarbonate ions are responsible for the 7K relaxation. In either case, the results imply that dipolar reorientation takes place either in the planes of cations or planes of anions since the 7K relaxation is only observed perpendicular and not parallel to the c-axis. At present, it is not clear how hydroxyl ions can be incorporated into the $(CO_3)^{-2}$ planes or how the associated proton motion could be restricted to the planes of anions or cations. However, it is straightforward to envision bicarbonate ions in the planes of the anions as it merely requires addition of a proton to a carbonate ion. The dipole reorientation could then take place via jumping of protons between carbonate ions adjacent to a substitutional monovalent ion. Because of the simplicity and plausibility of the model, the bicarbonate ions are favored as the source of the 7K relaxation at the present time.

The dynamics of the motion have several characteristics similar to that observed for the aluminum-hole center in α-quartz (Toulouse and Nowick, 1988). For example, it is apparent from Figure 6 that the relaxation time is very similar in the two materials but at higher temperatures the two curves deviate from one another. That type of behavior was also observed in quartz and the deviation at higher temperatures was attributed to defects.

Further, as mentioned above, the shape of the peaks is more Debye-like at the lowest temperatures as evidenced by the Cole-Cole parameter. Again, this was observed in α-quartz.

Other Relaxations

Four other relaxations were observed in various samples of calcite. The following discussion represents the best interpretation of each. It should be kept in mind that the association in each case is not strong.

121K Relaxation

The 121K relaxation was only observed for the Mexican sample. The NAA data indicate that there are four impurities which are unique to the Mexican sample. One possiblity which is interesting is zinc. The presence of zinc in the Mexican sample was confirmed by the XRF studies. Further, this relaxation is only observed parallel and not perpendicular to the c-axis. One way to associate this relaxation with zinc is if the zinc is substitutional and has equivalent positions off-center toward the planes of $(CO_3)^{-2}$ ions. This is reasonable because zinc is significantly smaller than calcium (Shannon 1976)

168K Relaxation

As is apparent from Figure 2, electric relaxation is observed in the Mexican and Gallatin Mt. samples in the vicinity of 168K both parallel and perpendicular to the optic axis. In fact, the dielectric loss perpendicular to the c-axis is complex consisting of at least two closely spaced peaks.

According to the NAA studies, there is only one impurity which exists only in the Mexican and Gallatin Mt. samples. The most likely possibility is magnesium. However, it is not clear how magnesium could give rise to a relaxation as there is no need for charge compensation. Again, magnesium is significantly smaller than calcium, so that one possibility is that magnesium occupies off-center sites toward interstitial positions. The reason is that there are two inequivalent interstitial positions near a calcium and thus the relaxation spectrum, particularly perpendicular to the optic axis, would be expected to be complex. However, a more likely possibility is that the relaxation is actually due to an unidentified substitutional-interstitial impurity complex.

21K Relaxation

Next, a small relaxation is observed at 21K in the Swakopmund sample though traces of the relaxation are observed in the Gallatin Mt. material. The NAA studies indicated the presence of an impurity unique to the Swakopmund sample. However, that impurity remains unidentified and hence the origin of the 21K relaxation in natural calcite remains undetermined.

220K Relaxation

Finally, there is a weak relaxation at about 220K which is observed in the Gallatin Mt. and Mexican materials. The origin of that peak is unclear.

CONCLUSIONS

It has been shown that the dielectric spectrum of calcite is characteristic of the material from a given region. Consequently, this technique is of geological interest as it has the potential for identifying the geographical origin of the material. In addition, while further work is necessary for demonstration, it may be that the dielectric spectrum is characteristic of the time of crystal formation and thus this technique may have applications in dating. These possibilities are particularly intriguing since dielectric spectroscopy can be nondestructive since plate-shaped samples are not an absolute necessity. In fact, dielectric spectrometers could be constructed to sample any part of a specimen of any shape. In any event, the results are of fundamental interest as a large number of dipolar defects have been catalogued and characterized, both regarding energetics and symmetry. By correlating the results with impurity analysis, infrared spectroscopy and previously reported thermoluminescence studies, several of the defects have been identified. Of most interest is the evidence that the 38K relaxation is associated with a yttrium - $(CO_3)^{-3}$ ion pair and that the 7K relaxation is attributed to proton motion perpendicular to the c-axis.

ACKNOWLEDGMENTS

This work was supported in part by the Naval Academy Research Council and the Naval Academy Trident Scholar Program. The work of two of the authors (MCW and JFL) was supported in part by a grant from

the National Science Foundation. The authors would like to thank Martin Nelson of USNA for carrying out the NAA studies of the samples and Dr. Suzanne Q. Lomax and Deborah Rendahl of the National Gallery of Art Scientific Laboratory for providing the x-ray fluorescence measurements.

REFERENCES

Andeen CG, Link D, and Fontanella, J (1977) Cluster-Associated Relaxations in Rare-Earth Doped Calcium Fluoride. Phys. Rev. B16: 3762-7.

Andeen CG, Fontanella JJ, Wintersgill MC, Welcher PJ, Kimble RJ Jr., and Matthews GE Jr., (1981) Clustering in Rare-Earth Doped Alkaline-Earth Fluorides. J. Phys. C: Solid St. Phys. 14: 3557-3574.

Bacquet G, Dugas J, Escribe C, Youdri L, and Belin C (1976) E.S.R. of CO_3^{3-}-Li^+ Centre in Irradiated Synthetic Single Crystal Calcite. J. de Phys. 36:427-9.

Calderon T, Aguilar M, and Coy-Yil R (1983) Relationship Between Blue Color and Radiation Damage in Calcite. Radiation Effects Letters 76: 187-191.

Cass J, Kent RS, Marshall SA, and Zager SA (1974) Electron Spin Resonance Absorption Spectrum of HCO_3^{2-} Molecule-Ions in Irradiated Single-Crystal Calcite. J. Mag. Res. 14: 170-181.

Figueroa DR, Fontanella JJ, Wintersgill MC, and Andeen CG (1984a) Association and Bound Motion in Alkali-Metal-Doped Cadmium Fluoride. Phys. Rev. B29: 5909-5919.

Figueroa DR, Fontanella JJ, Wintersgill MC, Chadwick AV, and Andeen CG (1984b) Dielectric Relaxation, Ionic Conductivity and Activation Volumes in Cubic Lead Fluoride Doped with Alkali-Metal Cations. J. Phys. C: Solid St. Phys. 17: 4399-4411.

Figueroa DR, Fontanella JJ, Wintersgill MC, and Andeen CG (1986) Electrical Relaxation in Cadmium Doped Cadmium Fluoride. Cryst. Latt. Defects and Amor. Materials. 15: 387-390.

Fontanella JJ and Andeen CG (1981) The Dielectric Spectrum of Erbium Doped CaF_2. J. Phys. C: Solid St. Phys. 14: 2451-2464.

Fontanella JJ, Wintersgill MC, Chadwick AV, Saghafian R, and Andeen CG (1981) Point Defect Activation Volumes in the Alkaline-Earth Fluorides. J.

Phys. C: Solid St. Phys. 14: 2451-2464.

Fontanella JJ, Wintersgill MC, Figueroa DR, Chadwick AV, and Andeen CG (1983) Anomalous Pressure Dependence of Dipolar Relaxation Times in Rare-Earth Doped Lead Fluoride. Phys. Rev. Letters 51: 1892-5.

Fontanella JJ, Wilson JJ, Smith MK, Wintersgill MC, Coughlin CS, Mazaud P, Greenbaum SG, Siddon RL (1991) Electrical Relaxation in Poly(propylene oxide) with and without Alkali Metal Salts. J. Poly. Sci.: Poly. Phys., submitted.

Kimble RJ Jr., Welcher PJ, Fontanella JJ, Wintersgill MC, Andeen CG (1982) Computer Modelling of Simple Point Defects in Rare-Earth-Doped Alkaline Earth Fluorides. J. Phys. C: Solid St. Phys. 15: 3441-3453.

Lapraz D and Iocconi P (1976) On Some Luminescent and Optical Properties of Synthetic Calcite Single Crystals. Phys. Stat. Sol. (a) 36:603-616.

de Lima JF, Yoshimura EM and Okuno E (1988) Thermoluminescence and Ionic Thermocurrent in Calcite. International Conf. on Defects in Insulating Crystals, Parma, Italy, 29 August-2 September 1988, abstract.

Link J, Wintersgill MC, Fontanella JJ, Bean VE, and Andeen CG (1981) Pressure Variation of the Low-Frequency Dielectric Constants of Some Anisotropic Crystals. J. Appl. Phys. 52: 936-9.

Marshall SA, McMillan JA, and Serway RA (1967) Electron Spin Resonance Absorption Spectrum of Y^{3+}-Stabilized CO^{3-} Molecular-Ion in Single-Crystal Calcite. J. Chem. Phys. 48:5131-5137.

Rao KS and Rao KV (1968) Dielectric Dispersion and its Temperature Variation in Calcite Single Crystals. Z. Phys. 216:300-6.

Shannon, RD (1976) Revised Effective Ionic Radii and Systematic Studies of Interatomic Distances in Halides and Chalcogenides. Acta Crst. A32: 751-767.

Shelby R, Fontanella J, and Andeen C (1980) The Low Temperature Electrical Properties of Some Anisotropic Crystals. J. Phys. Chem. Solids. 41: 69-74.

Smyth CP, (1955) **Dielectric Behavior and Structure**, (New York: McGraww-Hill).

Toulouse J and Nowick AS (1988) Dielectric Relaxation of the Aluminum-Hole Center in α-Quartz: An Example of Phonon-Assisted Tunneling. Phys. Rev. B37: 7070-7078

Table 1. ε''_{max} for relaxations in Swakopmund, Mexican (Iceland Spar), and Gallatin Mountain calcite at a frequency of 10^3 Hz and various orientations.

Sample (Cut)	**7K**	**13K**	**21K**	**38K**	**121K**	**168K**	**220K**
Mexican Iceland Spar							
#1(Cleave)	0.002			0.00017	0.022	0.0044	0.00006
#2(Cleave)	0.002			0.00008	0.001	0.004	0.0002
(⊥)	0.005	0.001				0.00067	
(∥)				0.005	0.0034	0.0042	
Gallatin Mountain							
#1(Cleave)	0.00045	0.00055	0.0005	0.0052		0.0018	0.0015
#2(Cleave)	0.0006	0.0014	0.00012	0.016		0.003	0.0002
#3(Cleave)	0.00043	0.00041	0.00005	0.007		Noise	
Noise							
Swakopmund							
#1(Cleave)		0.0002		0.0047			
#2(Cleave)		0.0037	0.0015	0.051			
#3(Cleave)		0.008	0.003	0.10			
#4(Cleave)		0.004	0.002	0.099			
(⊥)		0.022					
(∥)			0.011	0.4			

Table 2. Relaxation parameters for the principal relaxations observed in Swakopmund, Iceland Spar, and Gallatin Mt. calcite.

Sample(Cut)	T(K)	E(eV)	$\log_{10}(\tau_o(s))$	A(K)	α	B(K^{-1})
Gallatin(cleave)	7	0.0059	-8.01	0.0047	0.09	253
Mexican($\perp$)	7	0.0076	-9.20	0.0282	0.08	328
Gallatin(cleave)	12	0.0237	-12.02	0.034	0.07	-
Swakopmund($\parallel$)	38	0.0631	-12.26	37.0	0.13	-
Gallatin(cleave)	38	0.0628	-12.20	1.39	0.08	-
Mexican($\parallel$)	38	0.0634	-12.29	0.40	0.03	-
Mexican($\parallel$)	121	0.2201	-12.77	0.87	0.05	-
Mexican($\parallel$)	168	0.2907	-12.53	1.31	0.04	-
Gallatin(cleave)	168	0.298	-12.72	1.13	0.02	-

FIGURE CAPTIONS

Figure 1. ε'' vs. T(K) for various cleaved samples of calcite at a frequency of 10^3 Hz. Straight line segments connect the datum points. The samples are: solid - Swakopmund; short dash - Mexican; dash dot (chain) - Gallatin Mountain.

Figure 2. ε'' vs. T(K) parallel and perpendicular to the c-axis for Mexican calcite at a frequency of 10^3 Hz. Straight line segments connect the data points. The orientations are: solid - perpendicular to the c-axis; short dash - parallel to the c-axis.

Figure 3. ε'' vs. T(K) parallel and perpendicular to the c-axis for Swakopmund calcite at a frequency of 10^3 Hz. Straight line segments connect the datum points. The orientations are: solid - perpendicular to the c-axis; short dash - parallel to the c-axis.

Figure 4. ε'' vs. log(f(Hz)) at two temperatures for Swakopmund calcite cut to have a parallel orientation of the optic axis. Solid lines in the figure are the best-fit Cole-Cole (Equation (2)) curves. The temperatures are: Δ - 35.0K; square - 36.8K.

Figure 5. ln (τ) vs. 1000/T (1/K) for the 38K relaxation in the Swakopmund, Mexican, and Gallatin Mt. calcites. The solid line in the figure is the best-fit straight line (Arrhenius expression, Equation (5)) to the data for the Mexican material. The samples are: Δ - Swakopmund parallel to the c-axis; x - Gallatin Mt. cleave; square - Mexican parallel to the c-axis.

Figure 6. ln (τ) vs. 1000/T showing non-Arrhenius (quantum tunneling) behavior in both the Gallatin and Mexican (Iceland Spar) calcite. The solid lines are the best-fit theory based on Equation (6). The calcite samples are: square - Mexican (Iceland Spar); Δ - Gallatin.

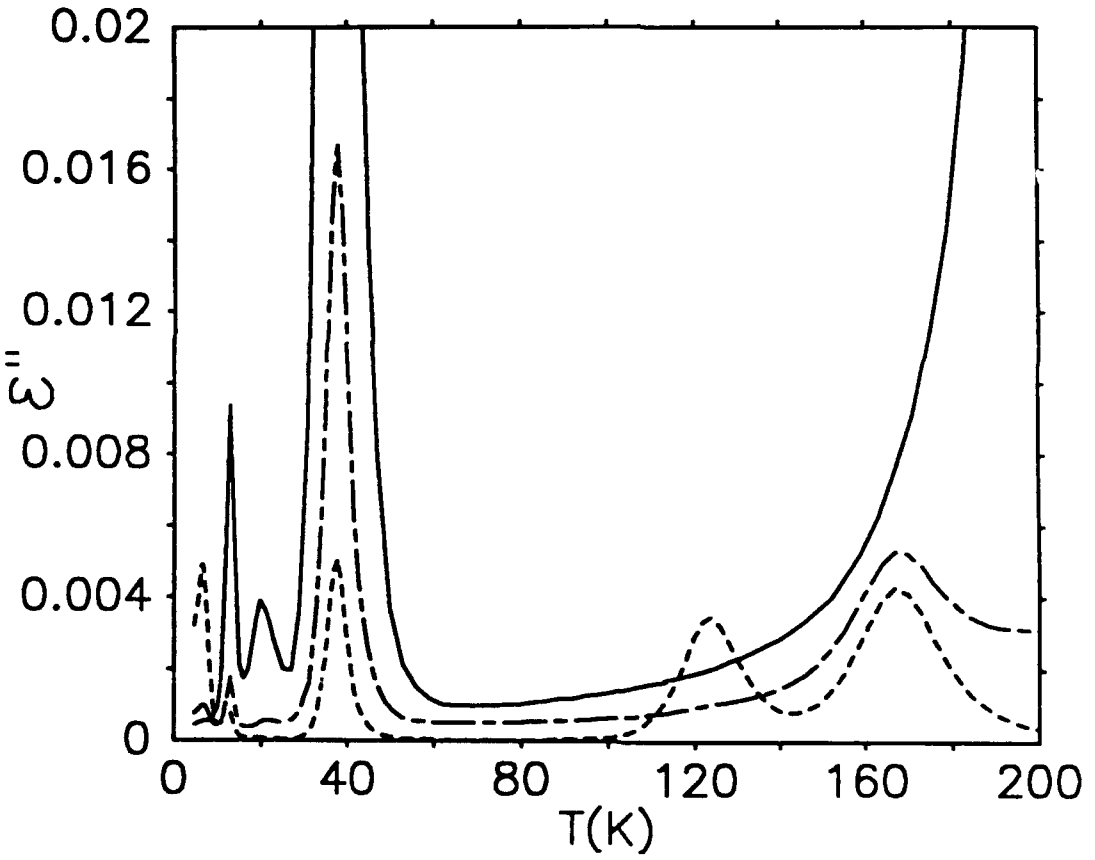
0.02
0.016
0.012
0.008
0.004
0
ω̃
0
40
80
120
160
200
T(K)

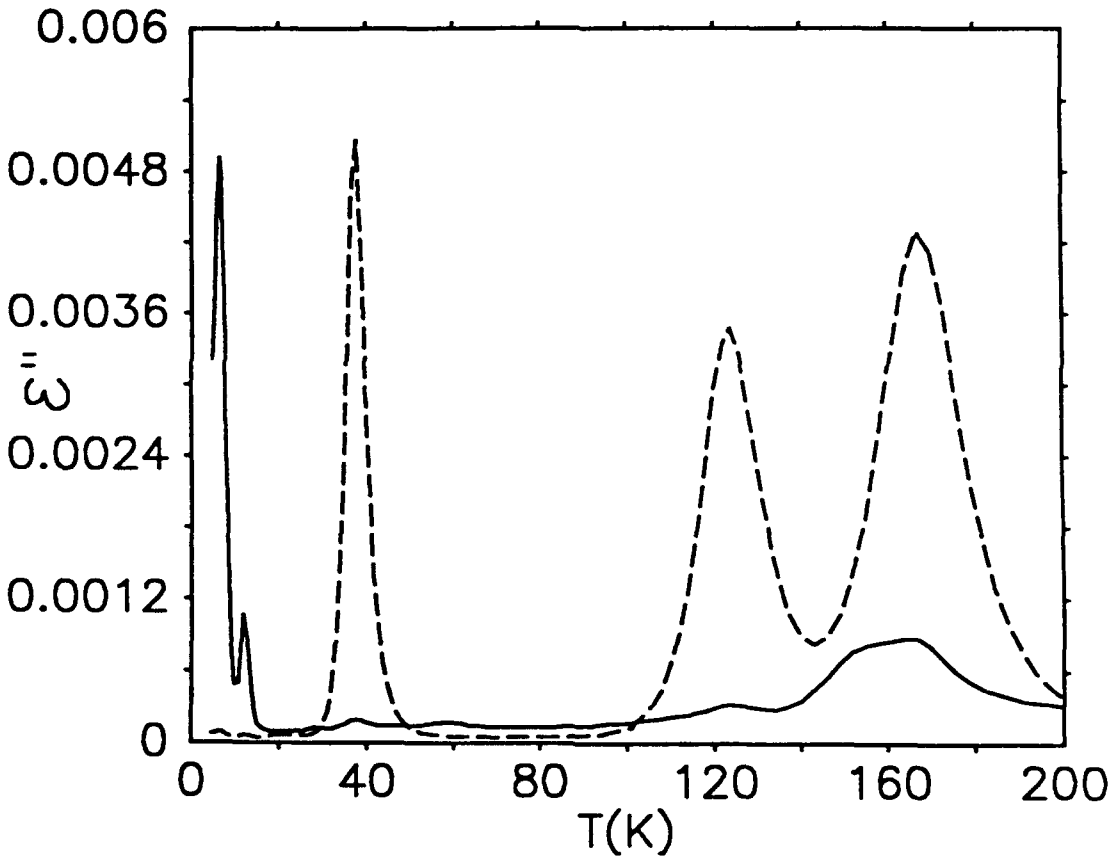
0.006
0.0048
0.0036
ω̃
0.0024
0.0012
0
0
40
80
120
160
200
T(K)

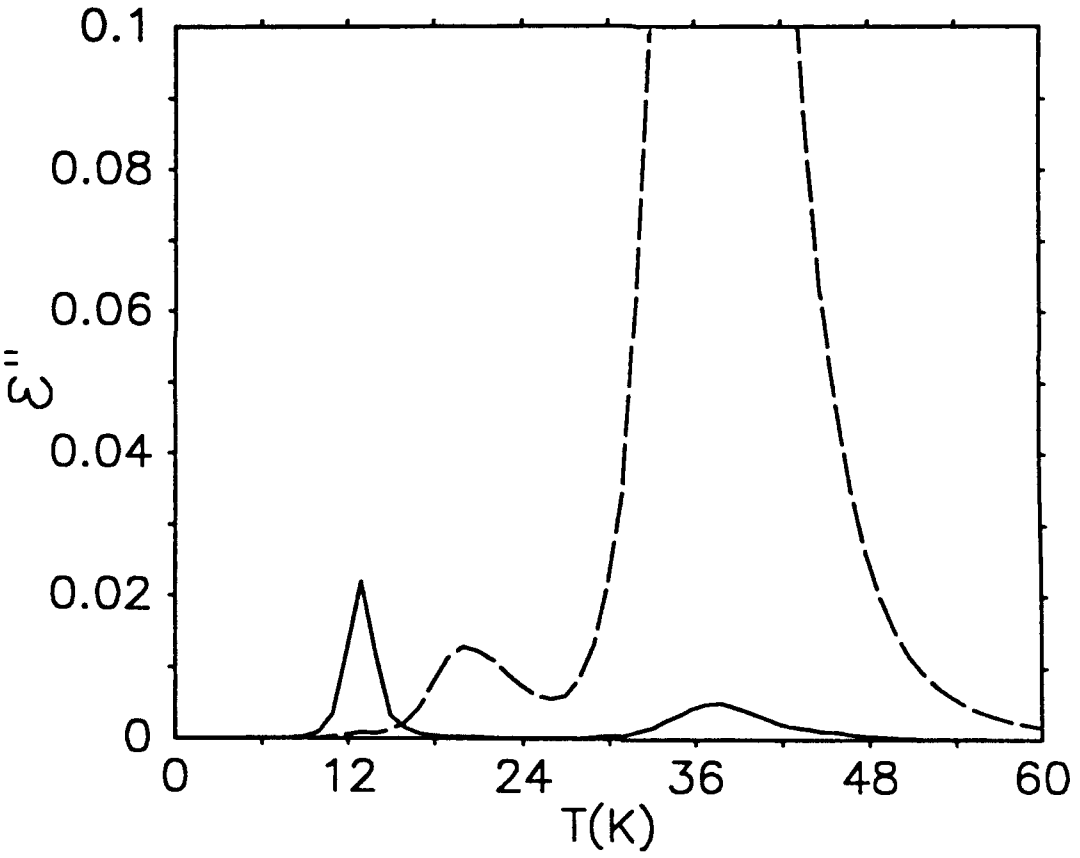
0.1
0.08
0.06
0.04
0.02
0
$\bar{\bar{\omega}}$
0
12
24
36
48
60
T(K)

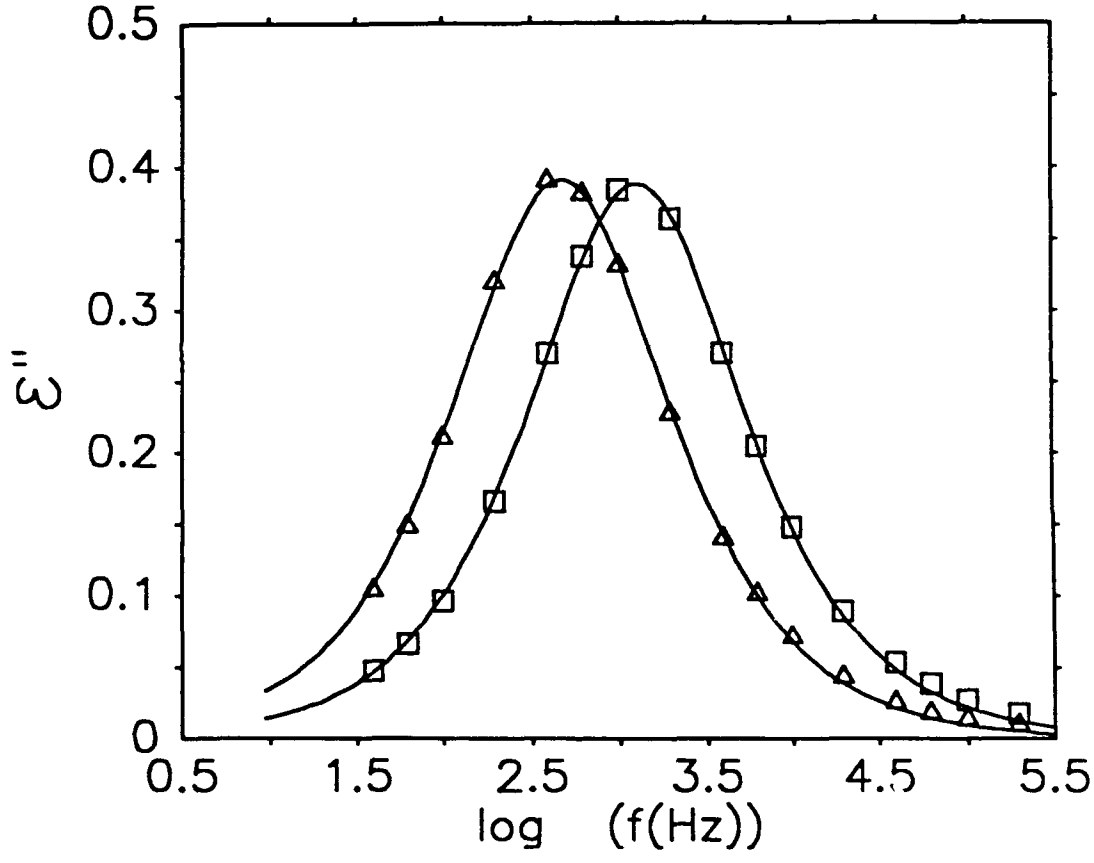
0.5
0.4
0.3
0.2
0.1
0
ε''
0.5
1.5
2.5
3.5
4.5
5.5
log (f(Hz))

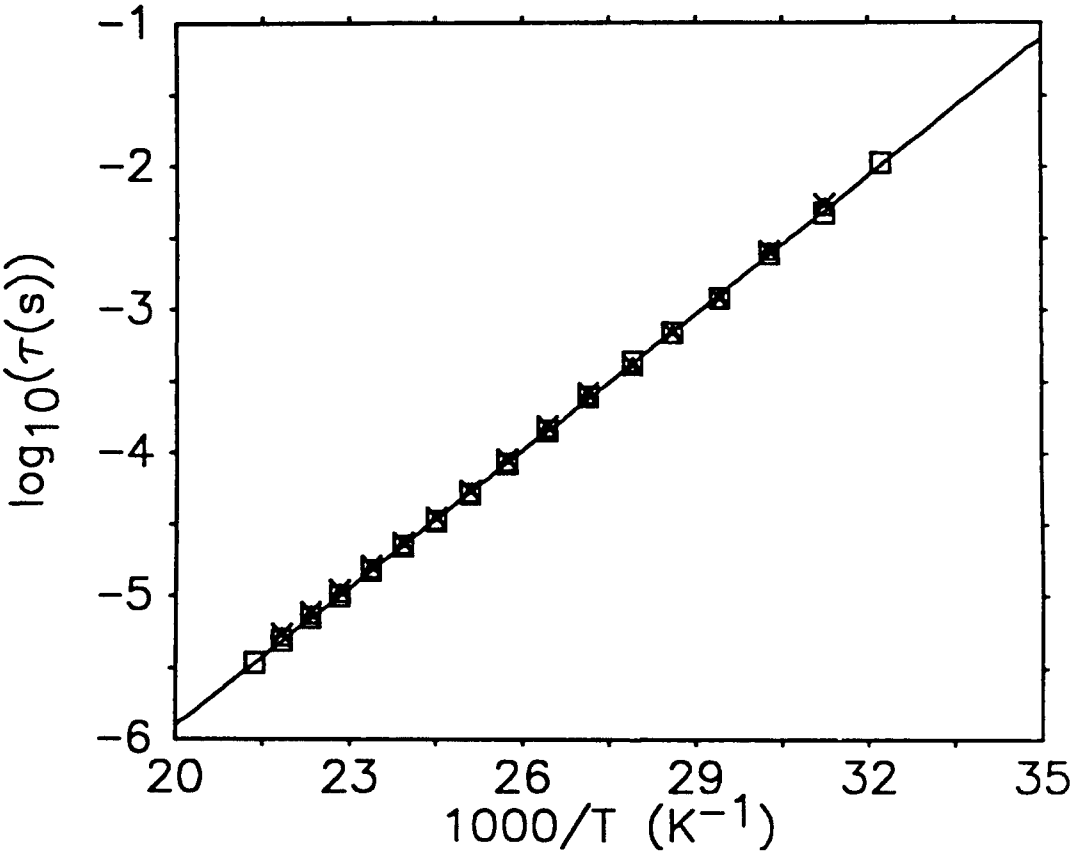
−1
−2
−3
−4
−5
−6
log10(τ(s))
20
23
26
29
32
35
1000/T (K−1)

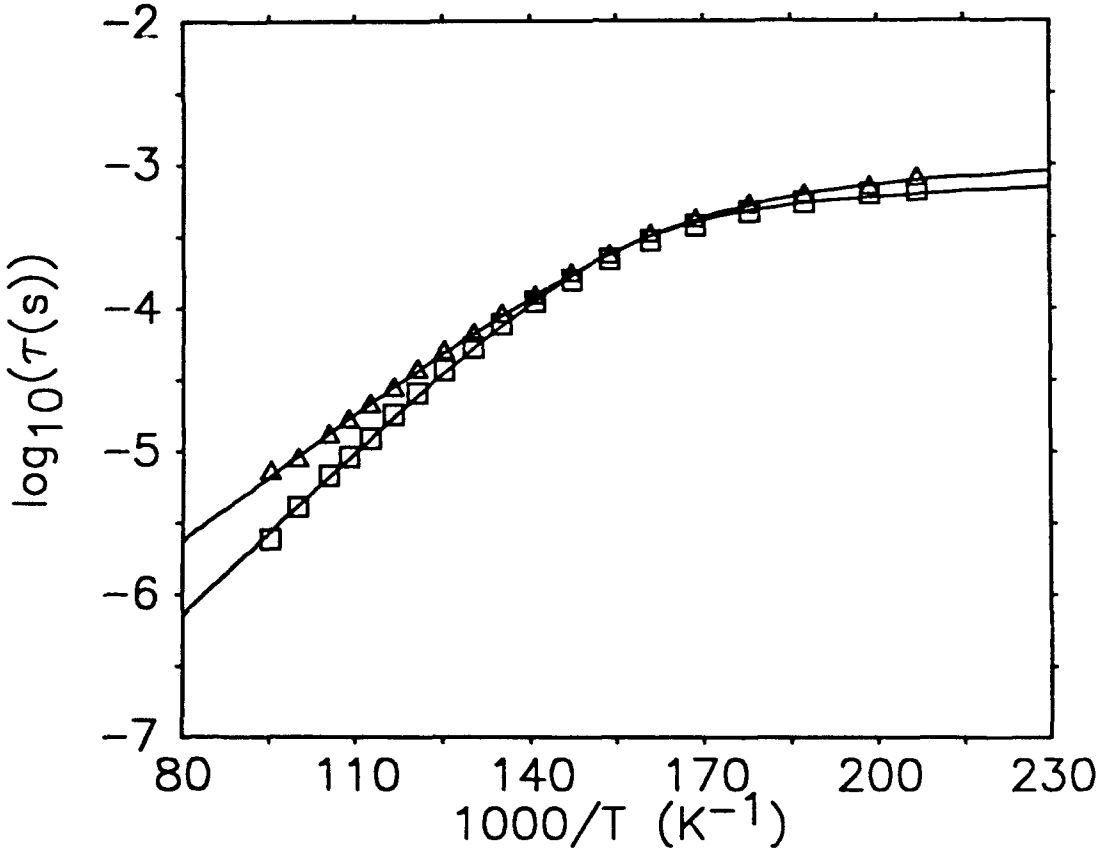
−2
−3
−4
−5
−6
−7
log10(τ(s))
80
110
140
170
200
230
1000/T (K−1)